

AMCoR

Asahikawa Medical University Repository <http://amcor.asahikawa-med.ac.jp/>

Traffic. (2013.2) 14(2):205–218.

Multiple sorting systems for secretory granules ensure the regulated secretion of peptide hormones.

Sun M, Watanabe T, Bochimoto H, Sakai Y, Torii S,
Takeuchi T, Hosaka M.

Multiple sorting systems for secretory granules ensure the regulated secretion of peptide hormones

Meng Sun^{1§}, Tsuyoshi Watanabe^{2§}, Hiroki Bochimoto², Yuko Sakai², Seiji Torii¹, Toshiyuki Takeuchi³, and Masahiro Hosaka^{1, 4,*}

¹ Department of Molecular Medicine, Institute for Molecular and Cellular Regulation, Gunma University, Maebashi, 371-8512, Japan

² Department of Microscopic Anatomy and Cell Biology, Asahikawa Medical University, Asahikawa, 078-8510, Japan

³ Administration office, Gunma University, Maebashi, 371-8510, Japan

⁴ Laboratory of Molecular Life Sciences, Department of Biotechnology, Akita Prefectural University, 010-0195, Japan

[§] These authors contributed equally to this work.

Running title: multiple granule sorting systems

Keywords: secretogranin III, secretogranin II, chromogranin A, cholesterol, peptide hormones, prohormone sorting, secretory granule

* Corresponding author:

Masahiro Hosaka

Laboratory of Molecular Life Sciences,

Division of Molecular and Cellular Biology

Department of Biotechnology,

Akita Prefectural University

Kaidobata-nishi 241-438, Shimo-Shinryo Nakano

Akita City, 010-0195, Japan

Tel: +81-18-872-1572

Fax: +81-18-872-1676

E-mail: mhosaka@akita-pu.ac.jp

Abstract

Prior to secretion, regulated peptide hormones are selectively sorted to secretory granules (SGs) at the trans-Golgi network (TGN) in endocrine cells. Secretogranin III (SgIII) appears to facilitate SG sorting process by tethering of protein aggregates containing chromogranin A (CgA) and peptide hormones to the cholesterol-rich SG membrane (SGM). Here, we evaluated the role of SgIII in SG sorting in AtT-20 cells transfected with small interfering RNA targeting SgIII. In the SgIII-knockdown cells, the intracellular retention of CgA was greatly impaired, and only a trace amount of CgA was localized within the vacuoles formed in the TGN, confirming the significance of SgIII in both the tethering of CgA-containing aggregates and the establishment of the proper SG morphology. Although the intracellular retention of proopiomelanocortin (POMC) was considerably impaired in SgIII-knockdown cells, residual ACTH/POMC was still localized to some few remaining SGs together with another granin protein, secretogranin II (SgII), and was secreted in a regulated manner. Biochemical analyses indicated that SgII bound directly to the SGM in a cholesterol-dependent manner and was able to retain the aggregated form of POMC, revealing a latent redundancy in the SG sorting and retention mechanisms, that ensures the regulated secretion of bioactive peptides.

Introduction

The secretory granules (SGs) in endocrine cells are cellular compartments in which peptide hormones, neuropeptides, and bioactive amines are selectively stored. The packaging of appropriate sets of soluble contents into SGs requires cooperation between aggregation- and receptor-mediated sorting processes in the trans-Golgi network (TGN) (1-3).

Classical members of the granin protein family, including chromogranin A (CgA), chromogranin B (CgB), and secretogranin II (SgII), automatically aggregate under conditions that mimic the intra-TGN milieu (4, 5). Therefore, the granin protein family has been regarded as integral to the aggregation-mediated sorting process and is thought to facilitate the condensation of peptide hormones and amines in the TGN and immature SGs (4, 6-10).

In parallel with the aggregation process in the TGN and immature SGs, micro-aggregates of secretory proteins and amines are tethered by peripheral or transmembrane receptors to the membrane domains destined for SGs. Loh and colleagues identified the first tethering receptor, membrane-associated carboxypeptidase E (CPE), based on the finding that proopiomelanocortin (POMC) is missorted to the constitutive secretory pathway in CPE-knockdown Neuro-2a cells and in the intermediate pituitary lobe of mice lacking CPE (Cpe^{fat} mice) (11). Other intragranular processing and modifying enzymes associated with cholesterol-rich lipid microdomains such as

prohormone converting enzymes (PC1/3 and PC2) and peptidylglycine alpha-amidating monooxygenase (PAM) might act as receptors that carry their own substrates to SGs (12).

Secretogranin III (SgIII) has been classified as a member of the granin protein family based on its biochemical properties and tissue distribution (3, 13). Among the granin protein family, SgIII exhibits a unique property in that it can bind specifically to both CgA and the cholesterol-rich membrane domain of the TGN (14, 15). Moreover, SgIII does not merely bind to CgA with a one-to-one stoichiometry; instead, it binds to CgA aggregates that include other bioactive peptides such as adrenomedullin, a major peptide hormone in chromaffin cells (10). Because of its multiple binding properties, SgIII could be a central component involved in the sorting of peptide hormones and amines to SGs. Besides in endocrine systems, SgIII has also been shown to direct secretory vesicle biogenesis in mast cells by interacting with CgA (16).

However, genetic ablation of SgIII in mice caused no apparent defects in terms of viability, fertility, or locomotion (17), despite the ubiquitous expression of SgIII in neuroendocrine cells and tissues (13, 14, 18-20). Similarly, genetic ablation (21, 22) or antisense RNA-mediated knockdown (23) of CgA in mice did not result in functional defects, with the exception of abnormal leakage of catecholamines from the adrenal medulla (21, 23). These studies suggest that endocrine tissues exhibit an alternate molecular pathway, possibly

involving other granin proteins, that compensates for the depletion of SgIII or CgA (22) and mediates the link between the aggregates and membranes destined for SGs.

To address the redundancy of the sorting mechanisms that ensures the regulated secretion of peptide hormones, we reduced the expression of SgIII in AtT-20 cells using an SgIII-targeted small interfering RNA (siRNA). AtT-20 cells are derived from corticotropes and secrete ACTH (adrenocorticotrophic hormone) in a regulated manner. We analyzed the changes induced by SgIII downregulation in the ultrastructure of the cells and in the sorting fidelity of ACTH and its precursor form, POMC, to SGs. We describe the overall effects of SgIII on SG biogenesis and evaluate the contribution of SgIII to ACTH/POMC sorting in AtT-20 cells.

Results

Overall effects of SgIII knockdown on hormone secretion in AtT-20 cells.

We have previously demonstrated that a small amount of SgIII efficiently targets CgA-containing hormone aggregates to SGs in endocrine cells (10, 14, 15). To address whether SgIII is crucial for the sorting of peptide hormones to SGs, we reduced SgIII expression in endocrine-derived cells. Because an exogenous SgIII-targeted siRNA (SgIII-siRNA) was more efficiently induced in AtT-20 cells than in MIN6 or PC12 cells (see Figure S1), AtT-20 cells were primarily used for further analyses.

Forty-eight hours after the transfection of AtT-20 cells with the SgIII-siRNA, the expression of SgIII level decreased to less than 5% of the levels in control cells transfected with non-targeting siRNAs. SgIII expression gradually recovered thereafter, reaching 35% of the control level at 120 h after transfection (Figure 1A). In contrast, the expression of a large form of CgA (97 kDa) slightly increased at 48 h after SgIII-siRNA transfection, and the expression of SgII, CPE, and α -tubulin remained at the same levels as in the untransfected wild type (WT) or control AtT-20 cells (Figure 1B, C).

When SgIII was knocked down in AtT-20 cells, immunocytochemical staining of ACTH/POMC was reduced and was principally confined to the perinuclear Golgi area at 48 h after siRNA transfection (Figure 2A, middle panels; Figure S2A, rows for #271si and #272si). In

addition to the staining in the Golgi, a limited number of granules were also immunostained with the anti-ACTH/POMC antibody. Consistent with the recovery of SgIII expression, granules containing SgIII were restored in the cells at 120 h after siRNA transfection (Figure 2A, lower panels), and ACTH/POMC is partially co-localized with SgIII in the granules, similar to the control cells (Figure 2A upper panels). Moreover, exogenous SgIII expression in SgIII-knockdown cells partially recovered ACTH/POMC localization to SGs (Figure S2A, panels at bottom).

The quantity of immunoreactive (ir)-ACTH within cells fluctuated consistently after SgIII-siRNA transfection; the ir-ACTH content decreased to one-fifth of the control level at 48 h after transfection and subsequently recovered to approximately 60% of the control level at 120 h after transfection (Figure 2B). Although the total intracellular ir-ACTH content was markedly reduced at 48 h after SgIII-siRNA transfection, residual ir-ACTH was still released in a regulated manner. No significant difference in the ratio of corticotropin-releasing hormone (CRH)-stimulated secretion to the basal level of ir-ACTH secretion was detected between SgIII-knockdown and control AtT-20 cells (Figure 2C). On the other hand, SgIII expression did not affect the transcription level of POMC, the precursor form of ACTH (Figure S2B). Although the translational level in SgIII KD cells was similar to that in control (Figure S2C, left panel), POMC that was immunoreactive with the anti-ACTH antibody (AB902) was secreted

as ir-ACTH into the media without any secretagogue, based on immunoprecipitation results (Figure S2C, right panel). These data indicate that certain amounts of the precursor POMC is constitutively secreted into the medium from SgIII KO cells, while residual intracellular ACTH, which is properly processed, is still secreted in a regulated manner in response to CRH (Figure 2C). It is also possible that some amounts of POMC could be degraded within the cell, but the proportion of the intracellular degradation of POMC in SgIII KO cells could not be evaluated.

SgIII knockdown shifted CgA from the regulated to the constitutive secretory pathway.

Next, we examined the retention of CgA, a specific binding partner of SgIII (14), in the SgIII-knockdown AtT-20 cells. Forty-eight hours after SgIII-siRNA transfection, the level of a large form of CgA (97 kDa) was slightly increased (to approximately 1.2-fold compared to the control levels), whereas that of a processed form, α -granin (20 kDa), was markedly decreased (Figure 1A, B). The immunocytochemical staining of CgA (Figure 3A, panels at the second row; Figure S3A) and CgB (Figure 3A, panels at the third row) was largely restricted to the Golgi area at 48 h after SgIII-siRNA transfection, whereas SgII, another granin family protein, was properly localized to the SGs at the periphery of the cell as well as in the perinuclear Golgi (Figure 3A, panels at the fourth

row; Figure S3B). As CgA was localized to both the SGs at the periphery of the cell and the perinuclear Golgi area in control AtT-20 cells (Figure 3A, panels at the first row), these findings suggest that the large form of CgA was neither properly delivered to peripheral SGs nor processed to α -granin in SgIII-knockdown cells; instead, the large form of CgA can be constitutively secreted not through the proper SGs.

The constitutive secretion of CgA from the SgIII-knockdown AtT-20 cells was confirmed in a pulse-chase experiment. In control AtT-20 cells, the quantity of radiolabeled CgA in the cell extract was more than 3.5-fold higher than that in the culture medium. This intracellular CgA was released into the medium in response to the specific secretagogue CRH. In SgIII-knockdown cells, however, half of the radiolabeled CgA was secreted into the culture medium in both the presence and absence of CRH (Figure 3B). On the other hands, SgII was targeted to the SGs and secreted in a regulated manner even in SgIII KO cells (Figure 3C). These morphological and biochemical findings support the hypothesis that SgIII is essential for the proper sorting and retention of CgA, but not SgII, in the SGs of endocrine cells.

SgIII knockdown induced vacuolation of CgA-containing compartments in the TGN.

Because the immunocytochemical findings presented in Figure 2A and Figure 3A suggested that ACTH/POMC and CgA accumulated atypically

in the Golgi area within SgIII-knockdown AtT-20 cells, we examined the ultrastructural changes in subcellular organelles by electron microscopy.

Forty-eight hours after SgIII-siRNA transfection, numerous vacuoles were observed near the nuclei of transfected (Figure 4B), but not control (Figure 4A), AtT-20 cells. Within these vacuoles, a small core of aggregates containing CgA and ACTH/POMC was frequently observed (open arrowheads in Figure 4D). The vacuoles may have originated from the TGN; immunofluorescence microscopy indicated a frequent occurrence of CgA-positive aggregates within the TGN46-positive compartment (Figure 5A, white arrowheads), and the immunogold particles indicative of TGN46 specifically labeled the membranes of the vacuoles (Figure 5B, arrows), in which a small core of aggregates containing CgA (Figure 5B, white arrowheads) could be observed. Furin, a processing enzyme primarily localized in the Golgi apparatus (24), was also detected in the vacuoles (Figure 5C).

Although the number of SGs was markedly reduced particularly at the tips of the cell processes in the SgIII-knockdown cells, a small number of round SGs with dense cores remained at the cell periphery (arrows in Figure 5E). In these residual SGs, SgII colocalized with ACTH/POMC (arrows in Figure 5F), whereas CgA formed small aggregates within the vacuoles (open arrowheads in Figure 5E).

The intracellular localization of ACTH/POMC and granins was confirmed via

subcellular fractionation (Figure 6). Subcellular organelles from either control or SgIII-knockdown AtT-20 cells were separated into 16 fractions using sucrose density gradient centrifugation. The fractions containing rough endoplasmic reticulum, cis-Golgi, synaptic vesicle-like microvesicles, mitochondria, and lysosomes were identified by immunoblotting with specific antibodies against calnexin, α -COP, synaptophysin, cytochrome C, and cathepsin D, respectively (15, 25). Because fractions #8-10 from the control AtT-20 cells contained all of the examined SG proteins (ACTH, CgA, CgB, SgII, SgIII, and CPE), these fractions were regarded as the 'SG fractions' in the control AtT-20 cells. While POMC and CPE were evenly distributed throughout all of these SG fractions, CgA, CgB, and SgII were unevenly distributed: CgA and CgB were predominantly localized in the heavier fraction (#10), whereas SgII was found in the lighter fraction (#8).

In SgIII-knockdown cells, the proteolytic processing of CgA to β -granin and POMC to ACTH was impaired (Figure 6), and the precursor form of CgA predominantly accumulated in lighter fractions (#2-4), distinct from the SG fractions of the control AtT-20 cells (#8-10). POMC was also detected in these lighter fractions (#2-4) but primarily remained in the SG fractions (#8-10). Additionally, CgB was also shifted to lighter fractions (#2-4), potentially reflecting co-aggregation with CgA (26). Based on the localization of furin and TGN46 in the fractions (#2-4), we concluded that the vacuolated trans-Golgi compartment containing the small

aggregated core of CgA and POMC accumulated in these lighter fractions (#2-4), as observed by electron microscopy (Figures 4, 5).

In contrast to CgA, SgII did not accumulate in the lighter vacuole fractions (#2-4) but instead remained in the normal SG fractions (#8-10) in SgIII-knockdown cells. These findings were consistent with the occurrence of a small number of SgII-containing SGs in SgIII-knockdown AtT-20 cells (arrows in Figures 5E, F) and the secretion assay results presented in Figure 3C, and suggest that SgII is correctly targeted to SGs via a mechanism distinct from the sorting mechanism that relies on SgIII and CgA (3).

SgII directly binds to the secretory granule membrane in a cholesterol-dependent manner.

As we demonstrated previously, SgIII binds specifically to the secretory granule membrane (SGM) in a cholesterol-dependent manner but does not bind to typical Triton X-100-resistant lipid rafts (15). Therefore, we investigated whether SgII binds to the SGM. To address the subgranular localization of SgII in SGs, the SG fractions (#8-10 in Figure 6) were lysed in a hypotonic solution and further divided by centrifugation into two fractions: a precipitated SGM fraction and a supernatant-soluble fraction. Immunoblotting showed that SgII accumulated in the SGM fraction (lane 1 of Figure 7A, B), similar to SgIII (15) and CPE (27). Because insolubility in detergent is a characteristic of lipids raft-associated proteins (28), we investigated whether SgII was associated with

lipid rafts using 1% Triton X-100. When the SGM was treated with 1% Triton X-100 for 30 min at 4°C, SgII and SgIII were detected in the soluble supernatant fraction (S), whereas CPE generally remained in the precipitated membrane fraction (P) (Figure 7A). These proteins were gradually dissociated from the SGM by washing using methyl- β -cyclodextrin (m CD), which selectively depletes cholesterol from membranes by the formation of a specific complex without affecting the phospholipid composition of the membrane (29). The binding properties of the SgII/SGM interaction were different from those of the SgIII interaction: after treatment with 100 mM m CD, SgII was still partially retained in the SGM fraction, similar to CPE, whereas SgIII was completely dissociated from the SGM (Figure 7B). In contrast to granins, phogrin, a trans-membrane protein on SGs, remained in the precipitated membrane fraction even after the SGM was treated with either Triton X-100 (Figure 7A) or m CD (Figure 7B).

To confirm the cholesterol-dependent binding of SgII to the SGM, we examined whether SgII could bind to [3 H]-labeled liposomes whose composition mimics the SGM (6.2 mol% PC, 17.7 mol% PE, 3.6 mol% PS, 1.0 mol% PI, 7.5 mol% SM, and 64 mol% cholesterol; 15, 27). As previously reported (15), SgIII bound to the SGM-type liposomes at pH 5.5, independent of the presence of 10 mM Ca^{2+} . In contrast, SgII 28-619 (encoding amino acid residues 28-619 of rat secretogranin II; see Materials and Methods) also bound to SGM-type liposomes but did not exhibit

an apparent pH or Ca^{2+} dependency (Figure 7C). The binding of SgII to [^3H]-labeled liposomes increased in parallel with the cholesterol content in the SGM, reaching the highest level at a 64 mol% cholesterol composition (Figure 7D). Together, these data show that SgII, SgIII, and CPE associate with the SGM in a cholesterol-dependent manner but display different binding properties.

POMC efficiently co-aggregated with SgII.

Because SgII was co-distributed with POMC in the remaining SGs within SgIII-knockdown AtT-20 cells (Figures 5, 6), we suspected that SgII sorts POMC to SGs independent of SgIII. To address this possibility, we examined the binding of SgII to POMC using an *in vitro* pull-down assay with GST-granins immobilized on glutathione beads. As previously reported (18), GST-SgIII 23-471 and CgA 1-444 pulled down POMC and POMC-derived peptides (Figure 8A, lanes 2 and 3). Interestingly, GST-SgII 28-619 also pulled down POMC and POMC-derived peptides (Figure 8A, lane 1), but GST-7B2 (SgV), which is also classified as a granin family protein, did not (Figure 8A, lane 4).

As we previously demonstrated, SgIII efficiently targets prohormone aggregates containing CgA to SGs (10). Because SgII self-aggregates in the weakly acidic, high- Ca^{2+} environment of SGs (5), we examined whether SgII co-aggregates with prohormones for efficient targeting to SGs. As shown in Figure 8B, the amount of aggregated POMC 27-235 increased in a concentration-dependent manner in the

presence of SgII or CgA. When incubated alone, the POMC fragment aggregated only weakly, even as its concentration increased. Therefore, SgII facilitates the aggregation of POMC and might tether the aggregates to the high cholesterol composition of membrane domain destined for the SGs in a cholesterol-dependent manner.

Discussion

Previous studies by our group demonstrated that SgIII plays a central role in the biogenesis of SGs in endocrine cells (14) by binding to CgA in core aggregates of soluble secretory products and to cholesterol-rich domains in the SGMs (3, 15). In this study, we showed that knocking down SgIII in AtT-20 cells induced prominent vacuolation in the TGN. Within the vacuoles, small cores of aggregates containing CgA were observed, however SgII, another granin family protein, was localized in the few remaining SGs with a normal morphology after SgIII knockdown. The localization of CgA in vacuoles of SgIII-knockdown cells confirmed that these two granins cooperate in SG biogenesis at the TGN.

The cholesterol-rich, lipid raft-like microdomains that accumulate specifically in the SGM are critical for the proper sorting and retention of the soluble constituents of SGs, including precursors of peptide hormones and granin family proteins (2, 30). The abundance of cholesterol in the SGM was first described based on biochemical analyses of subcellular fractions of chromaffin granules in the bovine adrenal medulla (31) and zymogen granules in the guinea pig pancreas (32; for review, see also 33), and visualized using filipin, a probe that forms a specific complex with cholesterol (34, 35). The cholesterol content of the SGM is estimated to be 65 mol% in the bovine pituitary neural lobe (27) and 37-45 mol% in PC12, AtT-20, and MIN6 cells (36). Although it is still not clear whether the

cholesterol-rich domains of the SGM are typical lipid rafts, which include glycosphingolipids, the cholesterol-rich membrane domains concentrated at the TGN likely attract peripheral proteins such as CPE (27, 37), PC2 (38), PC1/3 (39, 40), SgIII (15, 18), and SgII (in this study). These peripheral proteins associate with the membrane in a cholesterol-dependent manner and might carry their own soluble substrates or binding partner proteins, thereby retaining the proteins in the subcompartment of the TGN destined for the SGs (2, 3, 12).

In addition to the defect in the regulated secretion of CgA, the prominent changes in the ultrastructure of CgA-containing compartments near the TGN in SgIII-knockdown cells suggests that SgIII also affects the morphology of the TGN and/or SGs. Similar vacuolar changes of the TGN have been reported in AtT-20 cells grown in depleted medium containing lovastatin, an inhibitor of endogenous cholesterol synthesis (29). Depletion of cholesterol via lovastatin caused analogous changes in the SGs of mouse beta-cell-derived MIN6 cells. The SGs were considerably enlarged after lovastatin treatment, and the inner insulin-accumulating dense core drastically shrank or disappeared (41). These findings indicate that loss of cholesterol in the luminal leaflet of the membrane impairs the normal morphology of the TGN and/or SGs. Although it will be necessary to demonstrate the reduction of cholesterol in the vacuoles observed in the SgIII KO cells, the loss of SgIII might affect the retention

of cholesterol on the TGN, leading to the deformation of the CgA-containing SGs around the TGN.

In contrast to the vacuolation observed in the CgA-containing compartment, SGs containing SgII retained a normal appearance, displaying a dense core surrounded by a close-fitting membrane. Subcellular fractionation analysis also indicated that these two granins were potentially distributed in distinct sets of granules. Even after SgIII knockdown, SgII was distributed in the SG fraction as in the control cells, whereas CgA, CgB, furin, and TGN46 had shifted to lighter fractions.

Previous studies have demonstrated the distinct intracellular distributions of CgA and SgII. In the pituitary gonadotropes of male rats, CgA and SgIII are confined to large granules, whereas SgII is restricted to smaller granules (14, 42; see also Figure S4). When the expression of CgA in gonadotropes was suppressed by the continuous administration of estradiol, the large SGs containing CgA disappeared from the cells, whereas the smaller SGs containing SgII were retained, suggesting that these two types of SGs might be independently generated by distinct sorting mechanisms (43). After SgII knockdown in PC12 cells, the number of SGs was observed to be significantly decreased, but the SGs were not completely depleted, resulting in a partial defect in regulated secretion (44). Here we demonstrated that SgII binds to membrane lipids in a cholesterol-dependent manner, but its binding to the SGM appeared to be distinct from SgIII binding

to the SGM. This result also suggests that an alternative mechanism based on SgII facilitates SG formation, independent of the SgIII/CgA-mediated sorting mechanism. Although SgII contains no domains that are homologous to those in SgIII that are responsible for binding to the SGM identified by our previous study (15), helix–loop–helix motifs in the N- and C-terminal regions of SgII putatively function as alternative sorting domain(s) for targeting to SGs (45). Further studies should focus on the structural details for cholesterol binding domains of SgII and SgIII to determine the mechanism underlying the accumulation of cholesterol in the SG-budding region of the TGN.

Despite the existence of at least two distinct sorting systems for targeting granins to SGs, different granins colocalize within a single SG in most neuroendocrine cells, though not in male rat gonadotropes (for reviews on the tissue and cell distributions of granins; see 46, 47). Even in gonadotropes, intermediate SGs containing both CgA and SgII are appeared after stimulation (48). These findings suggest that distinct subsets of SGs become discernible only in special cells or functional states.

A parallel sorting mechanism for SGs could potentially explain not only the findings obtained in the SgIII-knockdown AtT-20 cells, but also those from mice lacking the granin genes. Mice with mutations in the SgIII gene presented no obvious changes in viability, fertility, or locomotion (17), even though SgIII was still widely expressed

in neuroendocrine cells and tissues (13-15, 19, 20). Similarly, CgA (21, 22, 49) and CgB (50) knockout mice do not exhibit a lethal phenotype. Taken together, these data suggest that redundancy in SG sorting mechanisms might ensure the continued regulation of peptide hormone secretion in the absence of a single granin protein. This hypothesis is further supported by the compensatory upregulation of other residual granins observed in the endocrine tissues of CgA and CgB knockout mice and by the elevation of the expression levels of SgIII and CgA observed in the pituitary gland of CPE-deficient mice (CPE^{fat/fat}) (18).

endocrine-derived cell lines.

In summary, this study investigated the versatile roles of SgIII in SG biogenesis and the proper sorting of CgA and its associated peptide hormone precursors. The dramatic reduction of SgIII expression in AtT-20 cells due to siRNA treatment revealed a latent redundancy in the sorting mechanisms of proteins destined for SGs. Under physiological conditions, granins and processing enzymes could function in parallel or, in some cases, cooperatively, to regulate SG biogenesis on cholesterol-rich platforms in the TGN. When any individual protein member in the platform is inactivated, the remaining proteins might compensate for the lost function to ensure the continued secretion of peptide hormones. The precise molecular and cellular mechanisms regulating the compensatory processes should be further analyzed in the context of both granin-deficient knockdown mice and

Materials and Methods

Cell culture

The mouse corticotrope-derived AtT-20 cell line was maintained in Dulbecco's modified Eagle's medium (DMEM) supplemented with 10% fetal bovine serum (FBS). The mouse pancreatic -cell-derived MIN6 cell line was cultured in DMEM with 15% FBS and 50 μ M 2-mercaptoethanol. Rat pheochromocytoma-derived PC12 cells were maintained in DMEM supplemented with 10% FBS and 10% horse serum with 50 ng/ml nerve growth factor.

Small interfering RNA transfection

Two siRNA constructs targeting mouse SgIII were synthesized by Integrated DNA Technologies, Inc. (IDT; Coralville, IA), and used to reduce the expression of SgIII in AtT-20 cells. The maximal knockdown efficiency was achieved using a combination of #270si (sense: rArUrArArGrArUrUrGrCrCrArCrArGrGrArUrUrUrArUGA; anti-sense: rUrCrArUrArArUrCrCrUrGrGrUrGrGrCrArArUrCrUrUrArUrGrG) and #271si (sense: rCrArArUrGrGrCrUrUrGrGrArArArGrGrArGrArArCrUrAAC; anti-sense: rGrUrUrArGrUrUrCrUrCrUrUrUrCrCrArArGrCrCrArUrUrGrGrA) siRNAs (see Figure 1B, Figure S2, and S3). AtT-20 cells were transfected with a 100 nM concentration of either mixture of the two SgIII-siRNA pools (#270si and #271si) or IDT's non-targeting siControl siRNA (control) in a 6-well (35-mm diameter) plate using LipofectAMINE 2000

(Invitrogen; Carlsbad, CA) at 24 h after the last passage. The effects of siRNA transfection on SgIII expression were assessed by immunoblotting and immunocytochemistry using an anti-SgIII antibody.

ACTH secretion assay

Prior to performing the ACTH secretion assay, AtT-20 cells were cultured in Krebs-Ringer bicarbonate glucose solution [15 mM HEPES (pH 7.4), 120 mM NaCl, 5 mM KCl, 2 mM CaCl₂, 1 mM MgCl₂, 24 mM Na₂HCO₃, 2.8 mM glucose, and 0.1% bovine serum albumin] for 2 h. To determine whether ACTH was released from cells by regulated secretion or by constitutive secretion, the medium was changed to fresh Krebs-Ringer bicarbonate glucose solution with or without 100 nM corticotropin releasing hormone (CRH; Calbiochem; Darmstadt, Germany). Following the secretion assay, ACTH was extracted from the cells in an acid-ethanol solution (70% ethanol and 0.18 M HCl), and immunoreactive (ir) ACTH was measured using an ACTH immunoradioactive assay kit (ACTH-IRMA; Mitsubishi Chemical Medience Corporation; Tokyo, Japan). After the secretion assay, the number of cells in each sample was counted, and the ACTH count was corrected accordingly. Note that this ACTH immunoradioactive assay kit (ACTH-IRMA) is highly specific for ACTH₁₋₃₉, and does not react with the precursor form, POMC, or related large peptide fragments (manufacturer's information; Mitsubishi Chemical Medience Corporation).

Antibodies

Rabbit polyclonal anti-SgIII (SgIII-C#6), anti-CgA (CgA-C#101), anti-SgII (SgII-#23), and anti-phogrin antibodies were prepared and characterized as described in our previous studies (SgIII, CgA and SgII antibodies: see ref. 19; phogrin antibody: see ref. 51). The following antibodies were purchased: anti-ACTH (AB902; rabbit polyclonal, Chemicon; Temecula, CA; mouse monoclonal, Biogenesis; Poole, UK), anti-CgA 94-130 (Y291; rabbit polyclonal, Yanaihara Institute Inc.; Fujinomiya, Japan), anti-CgA (611844; mouse monoclonal, BD Biosciences; San Jose, CA), anti-CgB (NB600-1516; rabbit polyclonal; Novus Biologicals; Littleton, CO), anti-furin (H-220; rabbit polyclonal, Santa Cruz Biotechnology, Inc.; Santa Cruz, CA), anti-SgII (sc-1491; goat polyclonal, Santa Cruz Biotechnology, Inc.; Santa Cruz, CA), anti-CPE (RDI-CARBYEabm; mouse monoclonal, Research Diagnostics, Inc.; North Acton, MA), anti- α -tubulin (T-5168; mouse monoclonal, Sigma-Aldrich; St. Louis, MO), and anti-TGN46 (ab76282; rabbit polyclonal, Abcam; Cambridge, MA). Secondary antibodies conjugated with fluorescent dyes (Alexa Fluor 488-, 594-conjugated donkey polyclonal anti-rabbit, mouse, goat IgG) or those with colloidal gold particles (10 and 15 nm in diameter) were purchased from Invitrogen and British Biocell International (Cardiff, UK), respectively.

Laser confocal microscopy

After the AtT-20 cells transfected with either the mixture of two SgIII-siRNA constructs (#270si and #271si) or the non-targeting siControl siRNA were cultured for 48 - 120 h, the cells were fixed with 4% paraformaldehyde in 0.1 M sodium phosphate buffer (pH 7.4) containing 4% sucrose for 30 min at 4°C and then permeabilized with high-salt TPBS (0.01 M sodium phosphate buffer, 0.5 M NaCl, 0.1% Tween 20, pH 7.3) containing 0.1% Triton X-100. The cells were incubated with the primary antibodies for 18 h at 4°C. For the second antibody reaction, the cells were incubated for 2 h at 20°C with an appropriate mixture of Alexa Fluor 488- and 594-labeled secondary antibodies. The immunostained cells were counterstained with DAPI and then mounted in 90% glycerol (vol/vol in PBS) containing 0.1% p-phenylenediamine dihydrochloride (Sigma-Aldrich), and observed with a laser scanning confocal microscope (LSM5Pascal; Carl Zeiss Microscopy GmbH, Jena Germany; or FV-1000D; Olympus, Tokyo, Japan).

Radiolabeling and Immunoprecipitation of

ACTH/POMC

siRNA-transfected AtT-20 cells in 6 wells were prewarmed in leucine-free DMEM for 1 h., and then radiolabeled with 35 μ Ci L-(4,5-³H) Leucine (Amersham Pharmacia Biotech, Piscataway, NJ) for 2 h. After radiolabeling, the cells were chased in normal DMEM for 1 h. Following the chase period, the culture media and cell extracts were immunoprecipitated with an ACTH antibody

(AB902), and subjected to the tritium measurement.

Radiolabeling and immunoprecipitation of CgA and SgII

siRNA-transfected AtT-20 cells were radiolabeled by incubation in a medium containing 0.2 mCi [³⁵S] methionine/cysteine (Amersham Pharmacia Biotech, Piscataway, NJ) for 2 h. The cells were further incubated in fresh DMEM with or without 100 nM CRH for 1 h. The culture media and cell extracts were then immunoprecipitated with either an anti-CgA (CgA-C#101) or an anti-SgII (SgII-#23) antibody, and the immunoprecipitated proteins were subjected to SDS-PAGE for fluorography. The relative intensities of the [³⁵S] signals of the appropriate band(s) for CgA or SgII were recorded and analyzed using the BAS-1800II system equipped with automatic integration software (Fujifilm, Tokyo, Japan). After the secretion assay, the cell number was counted for each condition, and the CgA or the SgII contents were corrected accordingly.

Immunoelectron microscopy

siRNA-transfected AtT-20 cells grown in 100-mm dishes were fixed with 2% glutaraldehyde/2% paraformaldehyde in 0.1 M phosphate buffer (PB) at pH 7.2 (15 min, 4°C), then gently removed from the dishes, and pelleted via centrifugation. After rinsing the pellets with 0.1 M PB containing 7.5% sucrose, the pellets were further fixed with 1% osmium tetroxide (OsO₄) in 0.1 M PB (pH 7.2) for

1 h at 4°C. The fixed pellets were then rinsed with 0.1 M PB (pH 7.2) containing 7.5% sucrose, dehydrated through a graded ethanol series, and embedded in Epon 812.

For immunocytochemical analyses, the AtT-20 cells grown in 100-mm dishes were fixed with 0.5% glutaraldehyde/0.5% paraformaldehyde in 0.1 M PB at pH 7.2 (15 min, 4°C), then gently removed from the dishes, and pelleted via centrifugation. The pellets were further fixed with 0.5% OsO₄ in 0.1 M PB (pH 7.2) for 20 min at 4°C, rinsed with 0.1 M PB containing 7.5% sucrose, and dehydrated three times with 70% ethanol containing 1% phosphotungstic acid (Wako Pure Chemical Co., Osaka, Japan) for 10 min at 4°C. After dehydration, the pellets were infiltrated three times into pure LR White resin (London Resin, Hampshire, UK) for 20 min each at 4°C and then placed in gelatin capsules with fresh LR White resin and polymerized for 24 h at 60°C.

Immunogold labeling was performed as previously described (19, 20). Briefly, ultrathin sections of the cell pellets were incubated with a mixture of primary antibodies against the antigens ACTH/POMC, CgA, SgII, furin, and TGN46 (see Figure Legends) for 12 h at 4°C. The localization of the antigens was visualized by incubating the sections with an appropriate mixture of secondary antibodies against different species (donkey polyclonal anti-rabbit, anti-mouse, and anti-sheep IgGs) conjugated with colloidal gold particles of distinct size (10 and 15 nm in diameter). The immunolabeled sections were contrasted using

saturated aqueous solutions of uranyl acetate and lead citrate and examined with a Hitachi H-7650 electron microscope (Hitachi; Tokyo, Japan).

Subcellular fractionation using a linear sucrose density gradient

AtT-20 cells in 100 mm plastic plates were detached by a 20-min incubation with PBS containing 10 mM EDTA at 37°C. The cells were then sedimented by light centrifugation and homogenized in buffer A (250 mM sucrose; 4 mM HEPES, pH 7.4; 1 mM MgCl₂; 0.005% DNase; and a protease inhibitor mixture [1 mg/ml each of aprotinin, leupeptin, and pepstatin A and 0.4 mM phenylmethylsulfonyl fluoride]). The homogenate was centrifuged at 3,000 x g for 2 min, and the resulting supernatant was recentrifuged at 5,000 x g for 15 min at 4°C. This post-nuclear supernatant was centrifuged at 26,000 x g for 15 min. The resultant pellet, representing the crude organelle fraction, was suspended in 0.8 ml of buffer A with 1.5 mM EDTA and layered onto a sucrose density gradient (20-70%, wt/vol), which was generated using a tilt tube in a Gradient Master (BioComp Instruments; NB, Canada) as previously described (15, 25). After centrifugation at 113,000 x g for 18.5 h at 4°C in a swing rotor, the gradients were fractionated by piston displacement from the top to the bottom using a Piston Gradient Fractionator (BioComp Instruments). The fractionated samples were concentrated for gel analysis after the addition of trichloroacetic acid to a 7.5% concentration and bovine serum albumin to a

0.01% concentration. Immunoblot analyses of these fractions were performed as previously described (15, 25).

In vitro binding assay

The following pGEX plasmids were used in this study: pGEXrSgII 28-619, encoding amino acids 28-619 of rat SgII; pGEXrSgIII 23-471, encoding amino acids 23-471 of rat SgIII; pGEXrCgA 1-444, encoding amino acids 1-444 of rat CgA (the rat CgA amino acid sequence is numbered by counting the first methionine as the -18th residue; 52); and pGEXr7B2 27-210, encoding amino acids 27-210 of rat 7B2. AtT-20 cells were solubilized with a buffer containing 50 mM MES (pH 5.5), 0.1 M NaCl, 1% Triton X-100, 10 mM CaCl₂, 1 mM EGTA, and a protease inhibitor cocktail and then centrifuged at 100,000 x g for 30 min at 4°C to obtain soluble extracts. Soluble extracts (20 µg) were incubated with continuous rotation for 12 h at 4°C together with 4 µg of one of the following proteins immobilized on glutathione beads: GST-SgII 28-619, GST-SgIII 23-471, CgA 1-444, or GST-7B2 27-210. The beads were then pelleted by centrifugation, and the proteins bound to the GST fusion proteins were subjected to SDS-PAGE followed by immunoblotting.

In Vitro Liposome-Binding Assay

A liposome-binding assay was performed essentially as previously described (15). Phospholipids (PC: phosphatidylcholine; PS: phosphatidylserine; PI: phosphatidylinositol; PE:

phosphatidylethanolamine; SM: sphingomyelin) and cholesterol were purchased from Avanti Polar Lipids (Alabaster, AL). [³H]-PC (1,2-dipalmitoyl, L-3-phosphatidyl [N-methyl-³H] choline; Amersham Pharmacia Biotech) was used as a radioactive marker. Lipid mixtures with the indicated compositions were dried under a stream of nitrogen gas and resuspended in 10 ml buffer A (50 mM HEPES-NaOH, pH 7.4, or 50 mM MES, pH 5.5, and 0.1 M NaCl). The mixture was then shaken for 1 min and sonicated for 30 sec using a probe sonicator. To remove aggregates, the liposome-containing mixture was centrifuged (10,000 x g for 10 min) prior to use. For a standard liposome-binding assay, 25 µg of recombinant proteins bound to glutathione agarose beads (10-µl wet volume) was used. The beads were pre-washed with buffer A containing 1.0 mM EGTA with or without 10 mM Ca²⁺, resuspended in 0.1 ml of the same buffer, and incubated with the [³H]-labeled liposomes for 10 min at room temperature with vigorous shaking. After the beads were pelleted by centrifugation (735 x g for 5 min) and washed three times with 1 ml of their respective incubation buffers, the radioactivity of the bead-bound liposomes was quantified by scintillation counting. All experiments were performed at least four times in quadruplicate.

In vitro aggregation assay

The recombinant rat proteins CgA 1-444, SgII 28-619, and POMC 27-235 were purified as previously described (18). Briefly, GST-fused CgA,

SgII, and POMC were cloned into the pGEX-6P-1 plasmid (Amersham Pharmacia Biotech), expressed in the BL21(DE3) strain, and then purified on glutathione beads. To remove the GST epitope, the GST-fused proteins were digested with pReScission protease (Amersham Pharmacia Biotech). The excised fragments of CgA, SgII, and POMC were retrieved by centrifugation each reaction mixture at 3,000 x g for 10 min.

To examine whether CgA or SgII could facilitate POMC aggregation, POMC (0.1 - 1 µg/ml) was incubated in a buffer (50 mM MES, pH 5.5, 0.1 M NaCl, and 10 mM CaCl₂) with either SgII (1 µg/ml) or CgA (1 µg/ml) for 2 h at 37°C. The reactions were then centrifuged at 100,000 x g for 30 min at 4°C to obtain aggregated protein precipitates. To prevent the nonspecific binding of proteins to the polycarbonate ultracentrifuge tubes, 0.01% Triton X-100 was added to the mixture (53). The pellet and supernatant fractions were subjected to SDS-PAGE and analyzed by immunoblotting with an anti-ACTH/POMC antibody. The quantities of POMC in the pellets (aggregated protein precipitates) and supernatants (residual soluble POMC) were estimated via densitometry from the immunolabeled band of the appropriate molecular weight for POMC using NIH image software.

Acknowledgements

The authors wish to thank M. Hosoi for valuable technical support.

This work was supported by Grants-in-Aid from the Japanese Ministry of Education, Culture, Sports, Science and Technology, the Joint Research Program of the Institute for Molecular and Cellular Regulation, Gunma University, and Akita Prefectural University President's Research Project Fund.

FOOTNOTE

Abbreviations used: SgIII, secretogranin III; SgII, secretogranin II; CgA, chromogranin A; CgB, chromogranin B; CPE, carboxypeptidase E; TGN, trans-Golgi network; SG, secretory granule; POMC, proopiomelanocortin; ACTH, adrenocorticotrophic hormone; CRH, corticotropin-releasing hormone; siRNA, small interfering RNA

References

1. Thiele C, Gerdes HH. and Huttner WB. Protein secretion: puzzling receptors. *Curr. Biol.* 1997;7:R496-500.
2. Kim T, Gondre-Lewis MC, Arnaoutova I, Loh YP. Dense-core secretory granule biogenesis. *Physiology (Bethesda)* 2006;21:124-133.
3. Hosaka M, Watanabe T. Secretogranin III: a bridge between core hormone aggregates and the secretory granule membrane. *Endocrine J.* 2010;57:275-286.
4. Gorr SU, Shioi J, Cohn DV. (1989). Interaction of calcium with porcine adrenal chromogranin A (secretory protein-I) and chromogranin B (secretogranin I). *Am. J. Physiol.* 1989;257:E247-E254.
5. Chanat, E., Huttner, W.B. Milieu-induced, selective aggregation of regulated secretory proteins in the trans-Golgi network. *J Cell Biol.* 1991;115:1505-1519.
6. Colomer V, Kicska GA, Rindler MJ. Secretory granule content proteins and the luminal domains of granule membrane proteins aggregate in vitro at mildly acidic pH. *J. Biol. Chem.* 1996;271:48-55.
7. Tooze SA. Biogenesis of secretory granules in the trans-Golgi network of neuroendocrine and endocrine cells. *Biochim. Biophys. Acta.* 1998;1404:231-244.
8. Glombik MM, Gerdes HH. Signal-mediated sorting of neuropeptides and prohormones: Secretory granule biogenesis revisited. *Biochimie* 2000;82:315-326.
9. Meldolesi, J., Chiergatti, E., Malosio, M.L. Requirements for the identification of dense-core granules. *Trends Cell Biol.* 2004;14:13-19.
10. Han L, Suda M, Tsuzuki K, Wang R, Ohe Y, Hirai H, Watanabe T, Takeuchi T, Hosaka M. A large form of secretogranin III functions as a sorting receptor for chromogranin A aggregates in PC12 cells. *Mol. Endocrinol.* 2008;22:1935-1949.
11. Cool DR, Normant E, Shen FS, Chen HC, Pannell L, Zhang Y, Loh YP. Carboxypeptidase E is a regulated secretory pathway sorting receptor: Genetic obliteration leads to endocrine disorders in Cpe^{fat} mice. *Cell* 1997;88:73-83.
12. Dikeakos JD, Reudelhuber TL. Sending proteins to dense core secretory granules: still a lot to sort out. *J. Cell Biol.* 2007;177:191-196.
13. Ottiger HP, Battenberg EF, Tsou AP, Bloom FE, Sutcliffe JG. 1B1075: a brain- and pituitary-specific mRNA that encodes a novel chromogranin/secretogranin-like component of intracellular vesicles. *J. Neurosci.* 1990;10:3135-3147.
14. Hosaka M, Watanabe T, Sakai Y, Uchiyama Y, Takeuchi T. Identification of a chromogranin A domain that mediates binding to secretogranin III and targeting to secretory granules in pituitary cells and pancreatic β -cells. *Mol. Biol. Cell* 2002;13:3388-3399.
15. Hosaka M, Suda M, Sakai Y, Izumi T, Watanabe T, Takeuchi T. Secretogranin III

- binds to cholesterol in the secretory granule membrane as an adapter for chromogranin A. *J. Biol. Chem.* 2004;279:3627-3634.
16. Prasad P, Yanagihara AA, Small-Howard AL, Turner H, Stokes AJ. Secretogranin III directs secretory vesicle biogenesis in mast cells in a manner dependent upon interaction with chromogranin A. *J. Immunol.* 2008;181:5024-5034.
 17. Kingsley DM, Rinchik EM, Russell LB, Ottiger HP, Sutcliffe JG, Copeland NG, Jenkins NA. (1990). Genetic ablation of a mouse gene expressed specifically in brain. *EMBO J.* 1990;9:395-399.
 18. Hosaka M, Watanabe T, Sakai Y, Kato T, Takeuchi T. Interaction between secretogranin III and carboxypeptidase E facilitates prohormone sorting within secretory granules. *J Cell Sci.* 2005;118:4785-4795.
 19. Sakai Y, Hosaka M, Hira Y, Harumi T, Ohsawa Y, Wang H, Takeuchi T, Uchiyama Y, Watanabe T. Immunocytochemical localization of secretogranin III in the anterior lobe of male rat pituitary glands. *J. Histochem. Cytochem.* 2003;51:227-238.
 20. Sakai Y, Hosaka M, Yoshinaga A, Hira Y, Harumi T, Watanabe T. Immunocytochemical localization of secretogranin III in the endocrine pancreas of male rats. *Arch. Histol. Cytol.* 2004;67:57-64.
 21. Mahapatra NR, O'Connor DT, Vaingankar SM, Hikim AP, Mahata M, Ray S, Staite E, Wu H, Gu Y, Dalton N, Kennedy BP, Ziegler MG, Ross Jr. J, Mahata K. Hypertension from targeted ablation of chromogranin A can be rescued by the human ortholog. *J. Clin. Invest.* 2005;115:1942-1952.
 22. Hendy GN, Li T, Girard M, Feldstein RC, Mulay S, Desjardins R, Day R, Karaplis AC, Tremblay ML, Canaff L. (2006). Targeted ablation of the chromogranin A (Chga) gene: Normal neuroendocrine dense-core secretory granules and increased expression of other granins. *Mol. Endocrinol.* 2006;20:1935-1947.
 23. Kim T, Zhang CF, Sun Z, Wu H, Loh YP. Chromogranin A deficiency in transgenic mice leads to aberrant chromaffin granule biogenesis. *J. Neurosci.* 2005;25:6958-6961.
 24. Mayer G, Boileau G, Bendayan M. Furin interacts with proMT1-MMP and integrin alphaV at specialized domains of renal cell plasma membrane. *J Cell Sci.* 2003;116:1763-1773.
 25. Hosaka M, Watanabe T, Yamauchi Y, Sakai Y, Suda M, Mizutani S, Takeuchi T, Isobe T, Izumi T. A subset of p23 localized on secretory granules in pancreatic beta-cells. *J Histochem. Cytochem.* 2007;55:235-245.
 26. Yoo SH. pH- and Ca²⁺-induced conformational change and aggregation of chromogranin B. Comparison with chromogranin A and implication in secretory vesicle biogenesis. *J. Biol. Chem.* 1995;270:12578-12583.
 27. Dhanvantari S, Loh PY. Lipid raft association of carboxypeptidase E is necessary for its function as a regulated secretory pathway

- sorting receptor. *J. Biol. Chem.* 2000;275:29887-93.
28. Harder T, Simons K. Caveolae, DIGs, and the dynamics of sphingolipid-cholesterol microdomains. *Curr Opin Cell Biol.* 1997;9:534-542.
29. Wang Y, Thiele C, Huttner WB. Cholesterol is required for the formation of regulated and constitutive secretory vesicles from the trans-Golgi network. *Traffic* 2000;1:952-962.
30. Tooze SA, Martens GJM, Huttner WB. Secretory granule biogenesis: rafting to the SNARE. *Trends Cell Biol.* 2001;11:116-122.
31. Blaschko H, Firemark H, Smith AD, Winkler H. Lipids of the adrenal medulla. Lysolecithin, a characteristic constituent of chromaffin granules. *Biochem. J.* 1967;104:545-549.
32. Meldolesi J, Jamieson JD, Palade GE. Composition of cellular membranes in the pancreas of the guinea pig. II. Lipids. *J. Cell Biol.* 1971;49:130-149.
33. Westhead EW. Lipid composition and orientation in secretory vesicles. *Ann N Y Acad Sci* 1987;493:92-100.
34. Orci L, Amherdt M, Montesano R, Vassalli P, Perrelet A. Topology of morphologically detectable protein and cholesterol in membranes of polypeptide-secreting cells. *Philos Trans R Soc Lond B Biol Sci* 1981;296:47-54.
35. Orci L, Montesano R, Meda P, Malaisse-Lagae F, Brown D, Perrelet A, Vassalli P. Heterogeneous distribution of filipin--cholesterol complexes across the cisternae of the Golgi apparatus. *Proc. Natl. Acad. Sci. U.S.A.* 1981;78:293-297.
36. Wang R, Hosaka M, Han L, Yokota-Hashimoto H, Suda M, Mitsushima D, Torii S, Takeuchi T. Molecular probes for sensing the cholesterol composition of subcellular organelle membranes. *Biochim. Biophys. Acta.* 2006;1761:1169-1181.
37. Zhang CF, Dhanvantari S, Lou H, Loh YP. Sorting of carboxypeptidase E to the regulated secretory pathway requires interaction of its transmembrane domain with lipid rafts. *Biochem. J.* 2003;369:453-460.
38. Blázquez M, Thiele C, Huttner WB, Docherty K, Shennan KIJ. Involvement of the membrane lipid bilayer in sorting prohormone convertase 2 into the regulated secretory pathway. *Biochem. J.* 2000;349:843-852.
39. Blázquez M, Docherty K, Shennan KI. Association of prohormone convertase 3 with membrane lipid rafts. *J. Mol. Endocrinol.* 2001;27:107-116.
40. Arnaoutova I, Smith AM, Coates LC, Sharpe JC, Dhanvantari S, Snell CR, Birch NP, Loh YP. The prohormone processing enzyme PC3 is a lipid raft-associated transmembrane protein. *Biochemistry* 2003;42:10445-10455.
41. Tsuchiya M, Hosaka M, Moriguchi T, Zhang S, Suda M, Yokota-Hashimoto, H, Shinozuka K, Takeuchi T. Cholesterol biosynthesis pathway intermediates and inhibitors regulate glucose-stimulated insulin secretion and

- secretory granule formation in pancreatic beta-cells. *Endocrinology*. 2010;151:4705-4716.
42. Watanabe T, Uchiyama Y, Grube D. Topology of chromogranin A and secretogranin II in the rat anterior pituitary: potential marker proteins for distinct secretory pathways in gonadotrophs. *Histochemistry* 1991;96:285-293.
 43. Watanabe T, Banno T, Jeziorowski T, Ohsawa Y, Waguri S, Grube D, Uchiyama Y. Effects of sex steroids on secretory granule formation in gonadotropes of castrated male rats with respect to granin expression. *Endocrinology* 1998;139:2765-2773.
 44. Courel M, Soler-Jover A, Rodriguez-Flores JL, Mahata SK, Elias S, Montero-Hadjadje M, Anouar Y, Giuly RJ, O'Connor DT, Taupenot L. Pro-hormone secretogranin II regulates dense core secretory granule biogenesis in catecholaminergic cells. *J Biol. Chem.* 2010;285:10030-43.
 45. Courel M, Vasquez MS, Hook VY, Mahata SK, Taupenot L. Sorting of the neuroendocrine secretory protein secretogranin II into the regulated secretory pathway—Role of N- and C-terminal alpha-helical domains. *J. Biol. Chem.* 2008;283:11807–11822.
 46. Wiedenmann B, Huttner WB. Synaptophysin and chromogranins/secretogranins—widespread constituents of distinct types of neuroendocrine vesicles and new tools in tumor diagnosis. *Virchows Arch B Cell Pathol Incl Mol Pathol* 1989;58:95-121.
 47. Winkler H, Fischer-Colbrie R. The chromogranins A and B: the first 25 years and future perspectives. *Neuroscience* 1992;49:497-528.
 48. Watanabe T, Jeziorowski T, Wuttke W, Grube D. Secretory granules and granins in hyperstimulated male rat gonadotropes. *J Histochem Cytochem* 1993;41:1801-1812.
 49. Montesinos MS, Machado JD, Camacho M, Diaz J, Morales YG, Alvarez delaRosa D, Carmona E, Castañeyra A, Viveros OH, O'Connor DT, Mahata SK, Borges R. The crucial role of chromogranins in storage and exocytosis revealed using chromaffin cells from chromogranin A null mouse. *J. Neurosci.* 2008;28:3350-3358.
 50. Díaz-Vera J, Morales YG, Hernández-Fernaud JR, Camacho M, Montesinos MS, Calegari F, Huttner WB, Borges R, Machado JD. Chromogranin B gene ablation reduces the catecholamine cargo and decelerates exocytosis in chromaffin secretory vesicles. *J. Neurosci.* 2010;30:950-957.
 51. Torii S, Saito N, Kawano A, Hou N, Ueki K, Kulkarni RN, Takeuchi T. Gene silencing of phogrin unveils its essential role in glucoseresponsive pancreatic beta-cell growth. *Diabetes* 2009;58:682–692.
 52. Iacangelo A, Okayama H, Eiden LE. Primary structure of rat chromogranin A and distribution of its mRNA. *FEBS Lett.* 1998;227:115-121.

53. Song L, Fricker LD. Calcium- and pH-dependent aggregation of carboxypeptidase E. *J. Biol. Chem.* 1995;270:7963-7967.

Figure Legends

Figure 1: Effects of SgIII-siRNA transfection on the expression of granin proteins.

(A) Cell lysates (20 μ g of protein per lane) from AtT-20 cells transfected with SgIII-siRNA (SgIII KD) or the non-targeting siControl (control) were subjected to SDS-PAGE and immunoblotting with an anti-SgIII (left upper panel) or anti-CgA 94-130 (left lower panel) antibody. The duration of incubation after SgIII-siRNA transfection is indicated above each lane. The relative quantities of SgIII are expressed as percentages of the control values (right panel; mean \pm s.e.m.; n = 5).

(B) Cell lysates (20 μ g of protein per lane) prepared from AtT-20 cells at 48 h after transfection with mock siRNA (WT), non-targeting siControl siRNA (control), SgIII-specific siRNA 1 (#270si), SgIII-specific siRNA 2 (#271si), or the combination of the two SgIII-specific siRNAs (SgIII KD; #270si and #271si) were separated via SDS-PAGE and analyzed by immunoblotting with anti-SgIII (left upper panel), anti-CgA 94-130 (left lower panel), anti-SgII (right upper panel), anti-CPE (right middle panel), and anti- α -tubulin (right lower panel) antibodies. (C) Based on the immunoblots shown in (B), the relative quantities of SgIII, the precursor form of CgA (97 kDa), the processed form of CgA (20 kDa; α -granin), SgII, CPE, and α -tubulin were evaluated by densitometry and are expressed as percentages of the control values (mean \pm s.e.m.; n = 5).

Figure 2: Effects of SgIII-siRNA transfection on the secretion of ACTH/POMC.

(A) AtT-20 cells were transfected with either the non-targeting siControl (control) or SgIII-specific siRNA (SgIII KD), and the immunocytochemical localization of SgIII and ACTH/POMC was observed at 48 h (control and SgIII KD 48 h) and 120 h (SgIII KD 120 h) after siRNA transfection using a confocal laser microscope (thickness of the optical slice; 0.5 μ m). Merged images obtained in DIC (Differential Interference Contrast) mode (gray scale) and of the immunocytochemical localizations of ACTH/POMC (green) and SgIII (red) and the DAPI nuclear counterstain (blue) at relatively low magnification are shown in the far left column of each set of panels. The ROIs (Regions Of Interest) indicated with a white square are shown at a higher magnification in the right adjacent column as merged images (merged) of DAPI stain (blue) and immunocytochemical localizations of ACTH/POMC (green) and SgIII (red). The localizations of ACTH/POMC and SgIII are also demonstrated separately as black/white images in the right two columns (ACTH/POMC [G] and SgIII [R], respectively). The asterisks in the panels of the 2nd and 3rd rows indicate the cells that express SgIII, even after SgIII-specific siRNA transfection. Note that only a few cells expressed SgIII and that most cells did not express detectable levels of SgIII at 48 h after siRNA transfection (2nd row, left panel), but the proportion of SgIII-expressing cells had apparently increased by 120 h after siRNA transfection (3rd row, left panel).

The cells indicated with white circles in the panels of the 3rd row did not exhibit restored SgIII expression, even at 120 h after siRNA transfection. Bars = 10 μ m. (B) The levels of immunoreactive (ir) ACTH in extracts of AtT-20 cells incubated for the indicated durations (24 - 120 h; SgIII KD) after SgIII-siRNA transfection were measured. The relative quantities of ir-ACTH in the cell extracts are expressed as percentages of the quantity of protein detected in AtT-20 cells transfected with the non-targeting siControl (control). The data are shown as the mean \pm s.e.m. (n = 5). (C) AtT-20 cells transfected with either the non-targeting siControl (control) or an SgIII-specific siRNA (SgIII KD) were cultured for the indicated durations (24 - 120 h) and then incubated in Krebs-Ringer buffer for an additional 2 h. The cells were subsequently stimulated via incubation with fresh Krebs-Ringer buffer \pm 100 nM CRH for 30 min, and the ir-ACTH levels in the cell extract and medium were separately measured using an ACTH immunoradioactive assay kit. The relative quantities of ir-ACTH in the cell extract (Cell) and medium (Med) are expressed as percentages of the total ir-ACTH (mean \pm s.e.m.; n = 5). Note that the ACTH immunoradioactive assay kit (ACTH-IRMA) is highly specific for ACTH₁₋₃₉, and does not react with the precursor form, POMC, or the related large peptide fragment (manufacturer's information; Mitsubishi Chemical Medience Corporation).

Figure 3: SgIII is necessary for the regulated secretion of CgA from AtT-20 cells.

AtT-20 cells were transfected with either the non-targeting siControl (control) or SgIII-specific siRNA (SgIII KD). (A) The immunocytochemical localization of CgA observed with a confocal laser microscope (thickness of the optical slice; 0.5 μ m) was compared with that of SgIII (1st row, control AtT-20 cells; 2nd row, SgIII-knockdown [SgIII KD] AtT-20 cells), CgB (3rd row of panels, SgIII KD) and SgII (4th row of panels, SgIII KD) at 48 h after siRNA transfection. In the far left column of each set of panels, the merged images obtained in DIC mode (gray scale) and of the immunocytochemical localizations of CgA (green) and another granin (red) and DAPI (blue) are shown at a relatively low magnification. The ROIs indicated with a white square on these panels are further demonstrated at the higher magnification in the right adjacent column as a merged image (merged) showing DAPI staining (blue) and the immunocytochemical localizations of two granins (CgA, green; other, red). The immunocytochemical localizations of each granin at the higher magnification are also separately demonstrated as black/white images in the right two columns (1st and 2nd rows, CgA [G] and SgIII [R]; 3rd row, CgB[R]; 4th row, SgII[R]). Note that the granular signals indicating CgA are co-localized with those of SgIII and scattered in the cytoplasm in the control AtT-20 cells (1st row, white arrowheads), while the immunocytochemical CgA signals are concentrated around the Golgi area near the cell nucleus in the SgIII-knockdown cells

(lower three rows). Note also that secretory granules contain SgII, but not CgA (4th row, white arrows), are observed in the cell periphery within the SgIII-knockdown cells, while the granules containing CgA in the same observed field (4th row, white arrowheads) are principally confined around the Golgi area. The asterisks in the left panel of the 2nd row indicate the cells that express a trace amount of SgIII, even after SgIII-specific siRNA transfection. Bars = 10 μ m. (B, C) The cells were pulse labeled for 1 h with [³⁵S]-methionine/cysteine at 48 h after siRNA transfection and then chased for 30 min in fresh medium with or without 100 nM CRH as a secretagogue. The samples precipitated from the cell extracts and chased medium with an anti-CgA (B) or an anti-SgII (C) antibody were separated via SDS-PAGE for analysis by fluorography (upper panels), and the radioactivity of the bands corresponding to CgA (B) or SgII (C) was quantified using BAS-1800II (Fujifilm) detection (lower panels). All experiments were independently repeated at least four times, and the relative quantities of precipitated CgA (B) or SgII (C) in the cell extracts (Cell) and media (Medium) are expressed as percentages of the total amount of CgA or SgII (mean \pm s.e.m.; n = 4).

Figure 4: Ultrastructural changes in the SgIII-knockdown AtT-20 cells.

The ultrastructural changes in AtT-20 cells 48 h after transfection of the non-targeting siControl (control; A, C) or an SgIII-specific siRNA (SgIII KD; B, D) were examined. The localizations of CgA and

ACTH/POMC were visualized with large (15 nm in diameter) and small (10 nm in diameter) colloidal gold particles, respectively (C, D). Note that the SgIII-knockdown AtT-20 cells contain numerous vacuoles (B) that were not present in the control AtT-20 cells (A). CgA and ACTH/POMC co-localized in a small aggregate core within each vacuole (open arrowheads; D), whereas in the control AtT-20 cells, they were found in secretory granules showing a normal morphology (arrow heads; C). Note that some secretory granules observed in the control AtT-20 cells contain ACTH/POMC but not CgA (C). Bars = 500 nm.

Figure 5: Intracellular localization of CgA, SgII, furin, and TGN46 in SgIII-knockdown cells.

(A) Immunocytochemical localizations of TGN46 and CgA at 48 h after SgIII-specific siRNA transfection (SgIII KD 48 h) observed with a confocal laser microscope (thickness of the optical slice; 0.5 μ m). Merged images obtained in DIC mode (gray scale) and of the immunocytochemical localizations of TGN46 (green) and CgA (red) and DAPI counterstaining (blue) at a relatively low magnification are presented in the far left panel. The ROI indicated with a white rectangle on the panel is further demonstrated at a higher magnification in the right adjacent panel as a merged image (merged) showing DAPI staining (blue) and the immunocytochemical localizations of TGN46 (green) and CgA (red). The localizations of TGN46 and CgA are also demonstrated separately as black/white images in the right two

panels (TGN46 [G] and CgA [R], respectively). Note that most of the immunocytochemical signals for CgA are located inside the TGN46-positive compartments in the SgIII-knockdown AtT-20 cells (white arrowheads). Bars = 10 μ m. (B-F) The immunocytochemical localizations of TGN46 (B), furin (C), and SgII (D-F) in control (D) and SgIII-knockdown (B, C, E, and F) AtT-20 cells were visualized using 15 nm immunogold particles. The localization of ACTH/POMC (C, F) and CgA (B, D, E) was visualized using 10 nm immunogold particles in ultrathin sections. The membranes of vacuoles in the SgIII-knockdown cells were immunocytochemically labeled with anti-TGN46 (B; arrows) and anti-furin (C) antibodies. These vacuoles occasionally contained a small core (open arrowheads) immunolabeled with anti-CgA (B) and anti-ACTH/POMC (C) antibodies. A vacuole containing a small core is shown at a higher magnification in the inset (C; asterisk). Although the gold particles indicating CgA were not localized in secretory granules but were instead detected in small core aggregates within the vacuoles of the SgIII-knockdown AtT-20 cells (open arrowheads in B, E), SgII remained in the secretory granules with normal morphologies (arrows in E and F). Note that secretory granules containing exclusively CgA (arrowheads) or SgII (arrow) can be also observed in the control AtT-20 cells (D). G: Golgi apparatus. Bars = 500 nm.

Figure 6: A shift in the distribution of organelles in the subcellular fractions of SgIII-knockdown AtT-20 cells.

Forty-eight hours after transfection with either a non-targeting siControl (control) or SgIII-specific siRNA (SgIII KD), crude organelle fractions prepared from the AtT-20 cells were subjected to sucrose density gradient centrifugation and divided into 16 fractions ranging from low to high (#1-#16) density. The fractionated samples were analyzed by immunoblotting with specific antibodies against SgIII, ACTH/POMC, CgA, CgB, SgII, CPE, furin, and TGN46 to determine the distributions of each protein among the different fractions. The cell homogenates were simultaneously analyzed as a starting material (H; 5 μ g). The “Secretory Granule Fraction” and “Vacuole-like Organelle Fraction” indicated with broken lines were defined based on the accumulation of ACTH in the control cells (fractions #8-#10) and the accumulation of furin and TGN46 in the SgIII-knockdown cells (fractions #2-#4).

Figure 7: Binding of SgII to the SGM.

The secretory granule fractions from AtT-20 cells (Figure 6; control) were hypotonically lysed and divided into secretory granule membrane (SGM) precipitate and supernatant fractions by centrifugation. The SGM fraction was incubated with either 1% Triton X-100 (TX-100) (A) or the indicated concentration of methyl- β -cyclodextrin (m β CD) (B). The precipitated (P) and soluble (S) fractions were obtained via ultracentrifugation. (A)

Effects of 1% Triton X-100 (TX-100) on the dissociation of SgII, SgIII, CPE, and phogrin from the SGM. Each fraction was subjected to SDS-PAGE and then analyzed by immunoblotting with specific antibodies against SgII, SgIII, CPE, and phogrin. Note that SgII and SgIII dissociated from the SGM into the supernatant in the presence of 1% TX-100 (upper and middle panels), whereas CPE largely remained in the SGM (lower panel). Phogrin, having a trans-membrane domain, remained in the SGM. (B) Effects of m CD on the dissociation of SgII, SgIII, CPE, and phogrin from the SGM. The concentration of m CD in the buffer is indicated above each lane. Note that increasing the concentration of m CD caused the dissociation of all three proteins from the SGM into the supernatant, but the concentration of m CD required for dissociation varied depending on the protein examined. SgIII partially dissociated from the SGM at 50 mM m CD and completely dissociated under 100 mM m CD (middle panel), whereas SgII and CPE remained partially at the SGM even in 100 mM m CD (upper and lower panels). Again, phogrin remained in the SGM fraction. (C) Assay to detect the binding of GST-fused SgII and SgIII to [³H]-labeled liposomes whose composition mimics that of the SGM (6.2 mol% PC, 17.7 mol% PE, 3.6 mol% PS, 1.0 mol% PI, 7.5 mol% SM, and 64 mol% cholesterol). The binding of the GST-fused SgII and SgIII to the SGM-type liposomes was tested under mildly acidic (pH 5.5) or neutral (pH 7.4) conditions, with (+) or without (-) 10 mM Ca²⁺. As a control, the

binding of GST to liposomes was also assayed. The values are given as the mean ± s.e.m. (n = 4). (D) Effect of the cholesterol composition of the lipid membrane on the binding of SgII to liposomes. To evaluate the effect of the cholesterol concentration on the binding of SgII, the binding of GST-fused SgII 28-619 to liposomes containing 0, 20, 40, or 64 mol% cholesterol was tested under the indicated conditions. All experiments were independently repeated at least four times (mean ± s.e.m.).

Figure 8: Binding and co-aggregation of POMC and granins.

(A) The GST fusion proteins GST-SgII 28-619, GST-SgIII 23-471, CgA 1-444, and GST-7B2 27-210 were individually immobilized on glutathione beads and incubated with an AtT-20 cell extract to pull down POMC. The precipitated POMC was analyzed by SDS-PAGE and immunoblotting using an anti-ACTH/POMC antibody. The cell extract (5 µg) was run in lane 5 (n = 5). (B) POMC 27-235 was incubated with or without 1 µg/ml SgII 28-619 or CgA 1-444 at the indicated concentrations in an intragranular environment with a pH of 5.5 and 10 mM Ca²⁺, and the pellet (P; precipitates of aggregated proteins) and supernatant (S) fractions were divided by centrifugation. The proteins in both fractions were further separated by SDS-PAGE and immunoblotted with an anti-ACTH/POMC antibody. The densities of the POMC bands were measured via densitometry using NIH image software. The

co-aggregated form of POMC is expressed as the ratio of POMC in the pellet to that in the supernatant plus the pellet (mean \pm s.e.m.; n = 5).

Supporting Information

Figure S1: Comparison of the transfection efficiency of exogenous siRNA among endocrine-derived cell lines.

The efficiency of siRNA transfection into AtT-20, MIN6, and PC12 cells was assessed by monitoring the expression of the co-transfected pEGFP vector. Forty-eight hours after co-transfection of the pEGFP vector and SgIII-specific siRNAs, the cells were imaged using fluorescent and phase contrast microscopy. Note that the proportion of AtT-20 cells expressing exogenous EGFP was much higher compared with PC12 and MIN6 cells. Bars = 100 μ m. PCI, phase contrast image.

Figure S2: Effects of SgIII on ACTH/POMC.

(A) Effects of transfection with individual SgIII-targeting siRNAs on the localization of ACTH/POMC. AtT-20 cells were transfected with the non-targeting siControl (control), #270si, #271si, or a combination of the #270si and #271si siRNAs (SgIII KD). Forty-eight hours after siRNA transfection, the localization of ACTH/POMC in control (1st row), #270si treated (2nd row), or #271si treated (3rd row) was visualized via immunofluorescence. Merged images of SgIII (green) and ACTH/POMC (red) staining are shown in the right column. The final row shows that

exogenous expression of rat SgIII rescues the ACTH/POMC localization in SgIII KD cells. SgIII KD cells were transfected with an expression construct that encodes rat SgIII (pcDNA3 rat Secretogranin III) 24 h after siRNA transfection, then cultured additional 24 h before being subjected to immunofluorescence assays. Bar = 20 μ m. (B) Northern blot of POMC to examine its transcriptional levels in control and SgIII KD cells 48 h after siRNA-transfection. Total RNA (10 μ g) from cells were analyzed in an agarose gel and hybridized with a ³²P-labeled cDNA probe for POMC and β -actin (left panel). The northern blot results were quantitatively evaluated by densitometry and graphed, taking the control as 100% (right panel). **C.** Metabolic labeling to measure translational activity for ACTH/POMC biosynthesis. Control and SgIII KD cells were labeled with [³H]-leucine for 2 h and chased for 1 h. The culture media and cell extracts were precipitated by an anti-ACTH antibody (AB902), and then counted by scintillation counter. The radioactive signals of total immunoprecipitated ACTH/POMC were standardized to the cell number and graphed assuming the control as 100% (left panel; mean \pm s.e.m.; n = 4). The relative quantities of precipitated ACTH/POMC in the cell extracts (Cell) and media (Medium) were also measured separately and expressed as percentages of the total amount of ACTH/POMC for each group of cells (right panel; mean \pm s.e.m.; n = 4). All experiments were independently repeated at least four times.

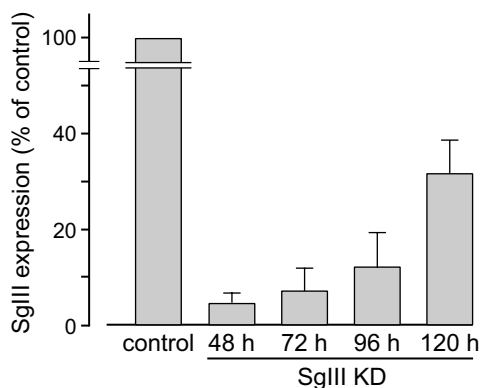
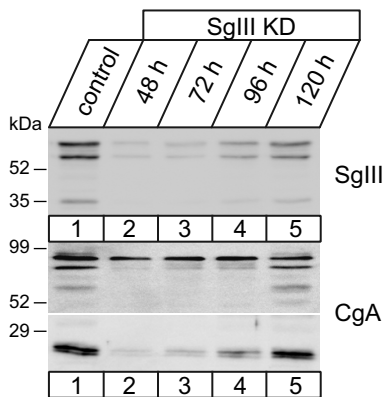
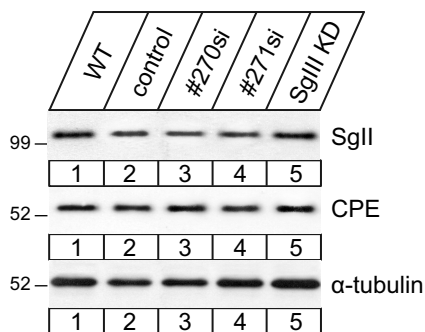
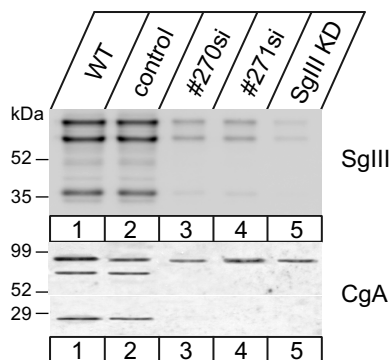
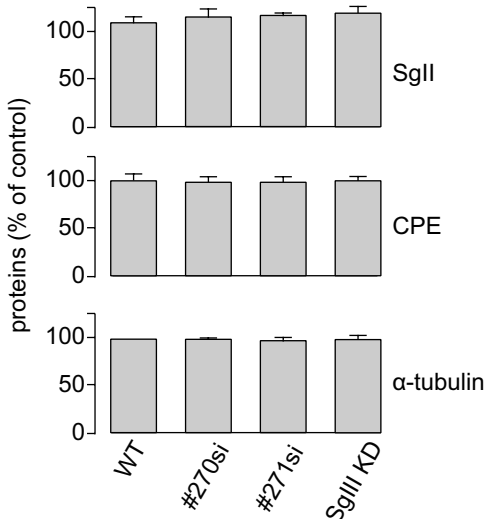
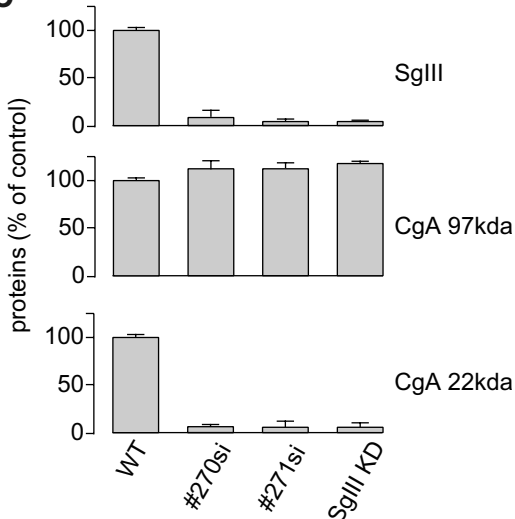
Figure S3: SgII localized at secretory granules in the absence of SgIII.

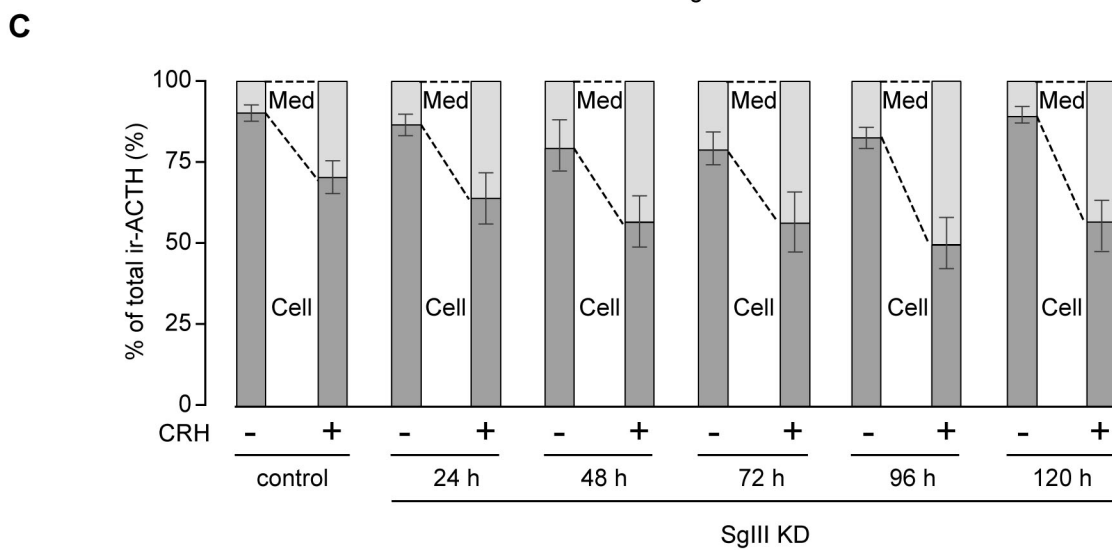
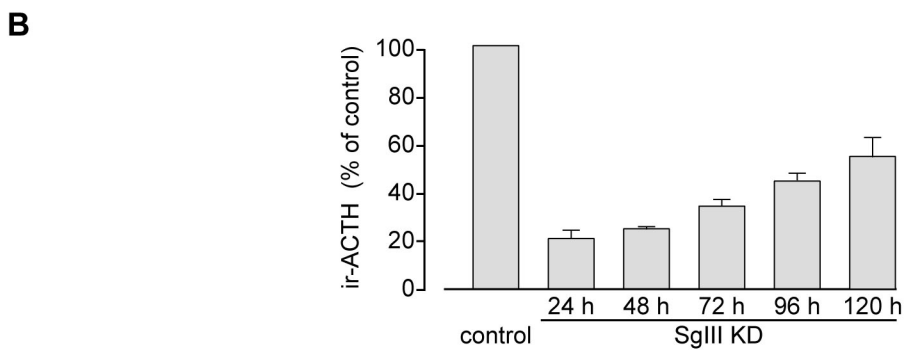
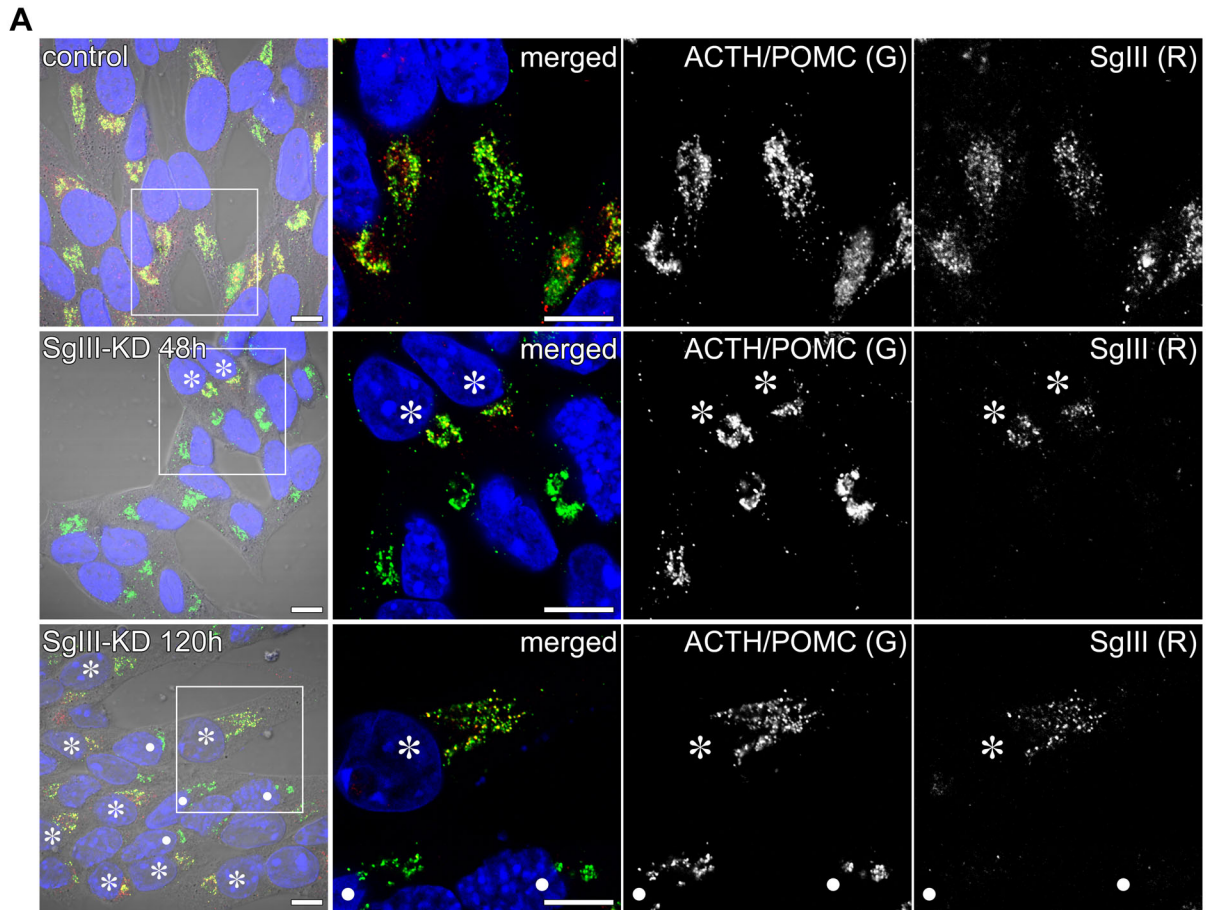
AtT-20 cells were transfected with the non-targeting siControl siRNA (control), #270si, #271si, or a combination of the #270si and #271si siRNAs (SgIII KD). (A) The immunocytochemical localization of SgII (green) and CgA (red) was visualized at 48 h after siRNA transfection. Detailed analyses of the AtT-20 cells transfected with a combination of these two SgIII-specific siRNAs (SgIII KD) are presented in Figure 3A. Bar = 20 μ m. (B) The immunocytochemical localization of SgII (green) and SgIII (red) was visualized at 48 and 120 h after SgIII-specific siRNA transfection. Merged images of SgII and SgIII staining are shown in the right column of each set of panels. Bar = 20 μ m.

Figure S4: Immunocytochemical localization of CgA, SgII, and SgIII in male rat pituitary gonadotropes.

Gonadotropes were identified by immunolabeling with an antibody against the β subunit of luteinizing hormone (LH ; 5 nm gold particles). (A) The localization of CgA and SgII in a pituitary gonadotropes was visualized using 15 and 10 nm colloidal gold particles conjugated with the appropriate secondary antibodies, respectively. Note that CgA was restricted to large secretory granules (arrows), whereas SgII was confined to smaller secretory granules (closed arrowheads). An intermediate type of secretory granule

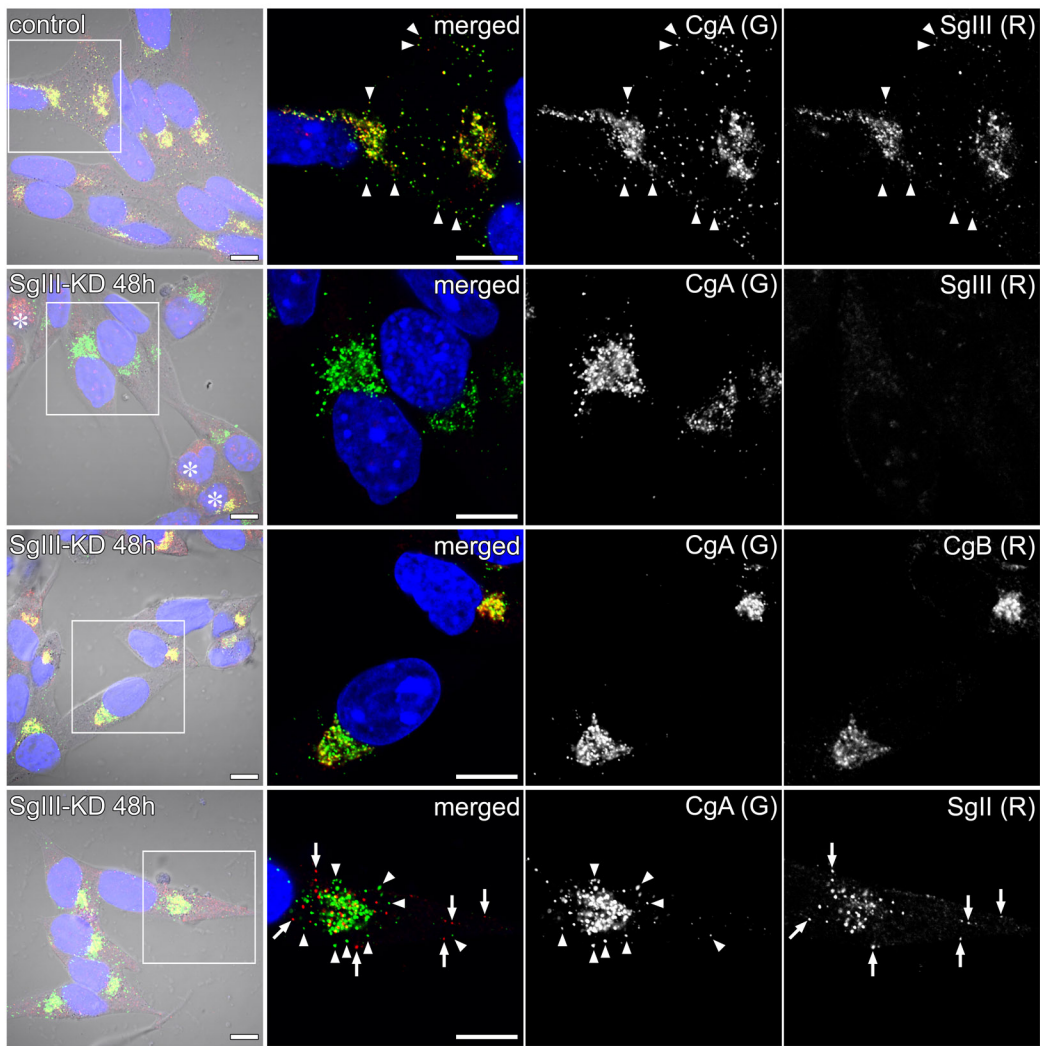
containing both CgA and SgII was occasionally observed (open arrowheads), but CgA and SgII were still separated in the peripheral and core regions of the intermediate granules. (B) SgIII (15 nm gold particles) was localized with CgA (10 nm gold particles) in the large granules (200-250 nm in diameter; arrows) but (C) not with SgII (10 nm gold particles) in the smaller granules (100-150 nm in diameter; closed arrowheads). For a more detailed description of the materials and methods, see ref. 14 and 19. Bar = 500 nm.

A**B****C**

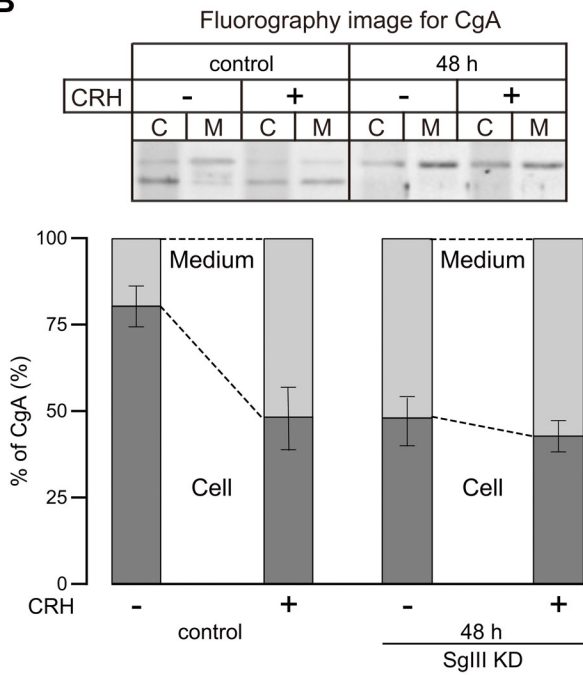


Sun et al., Figure 2

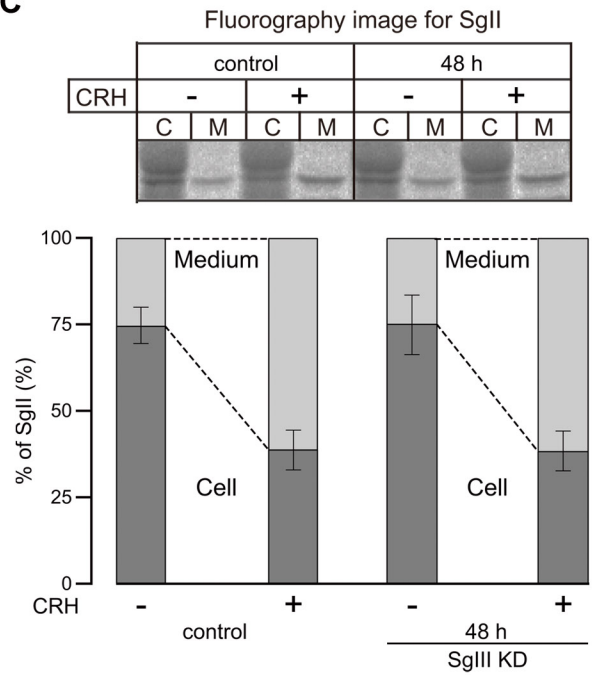
A

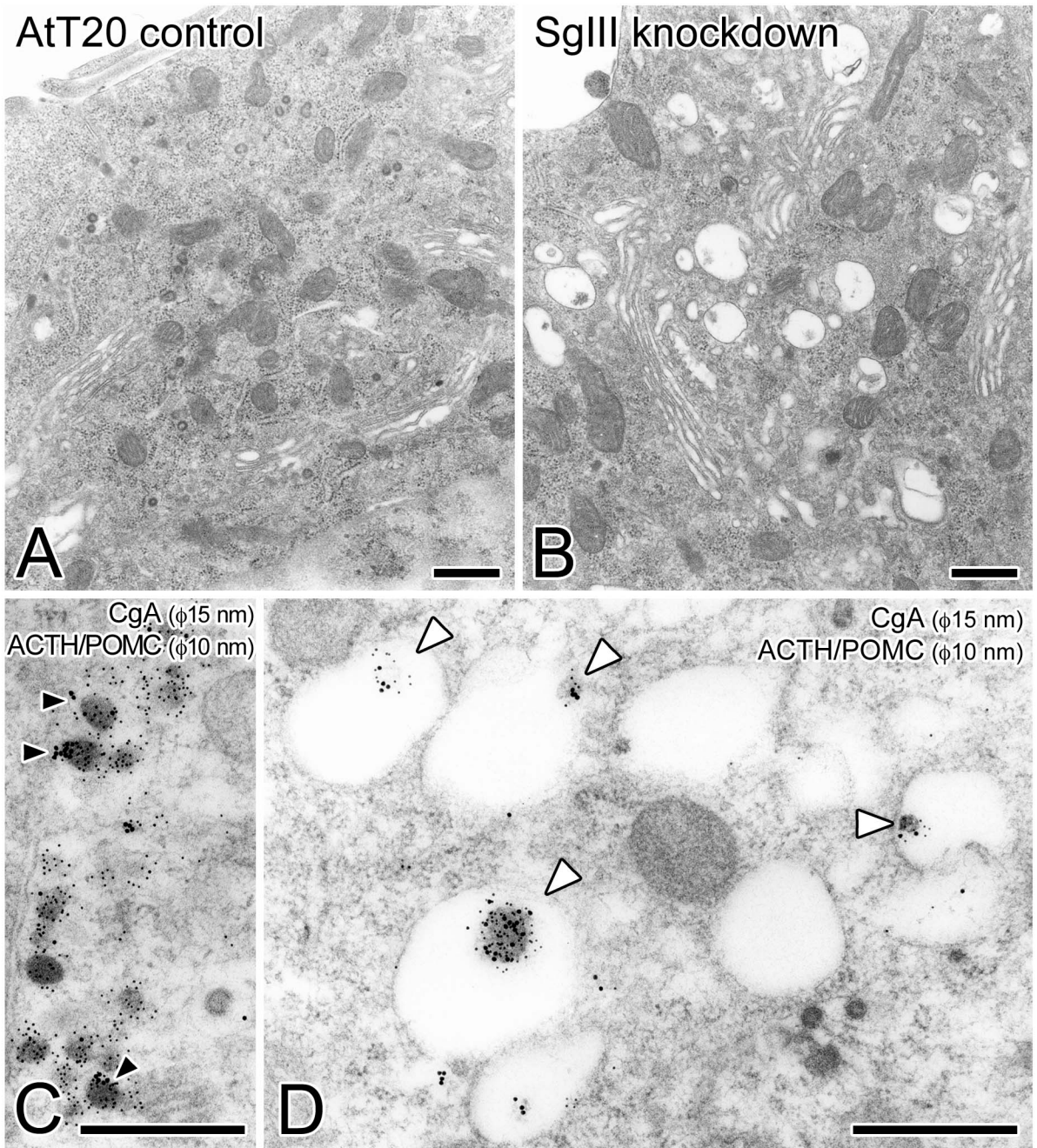


B

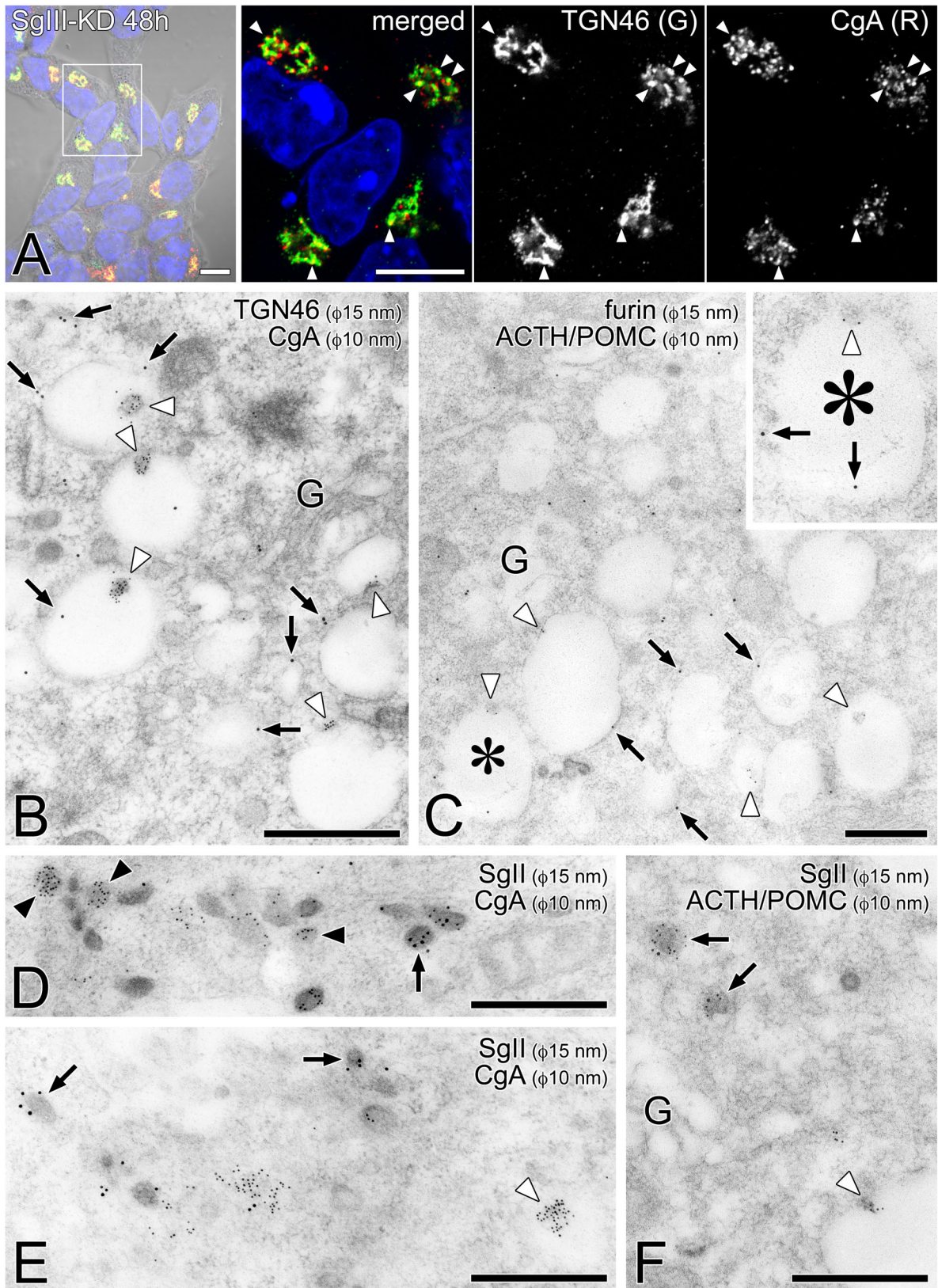


C

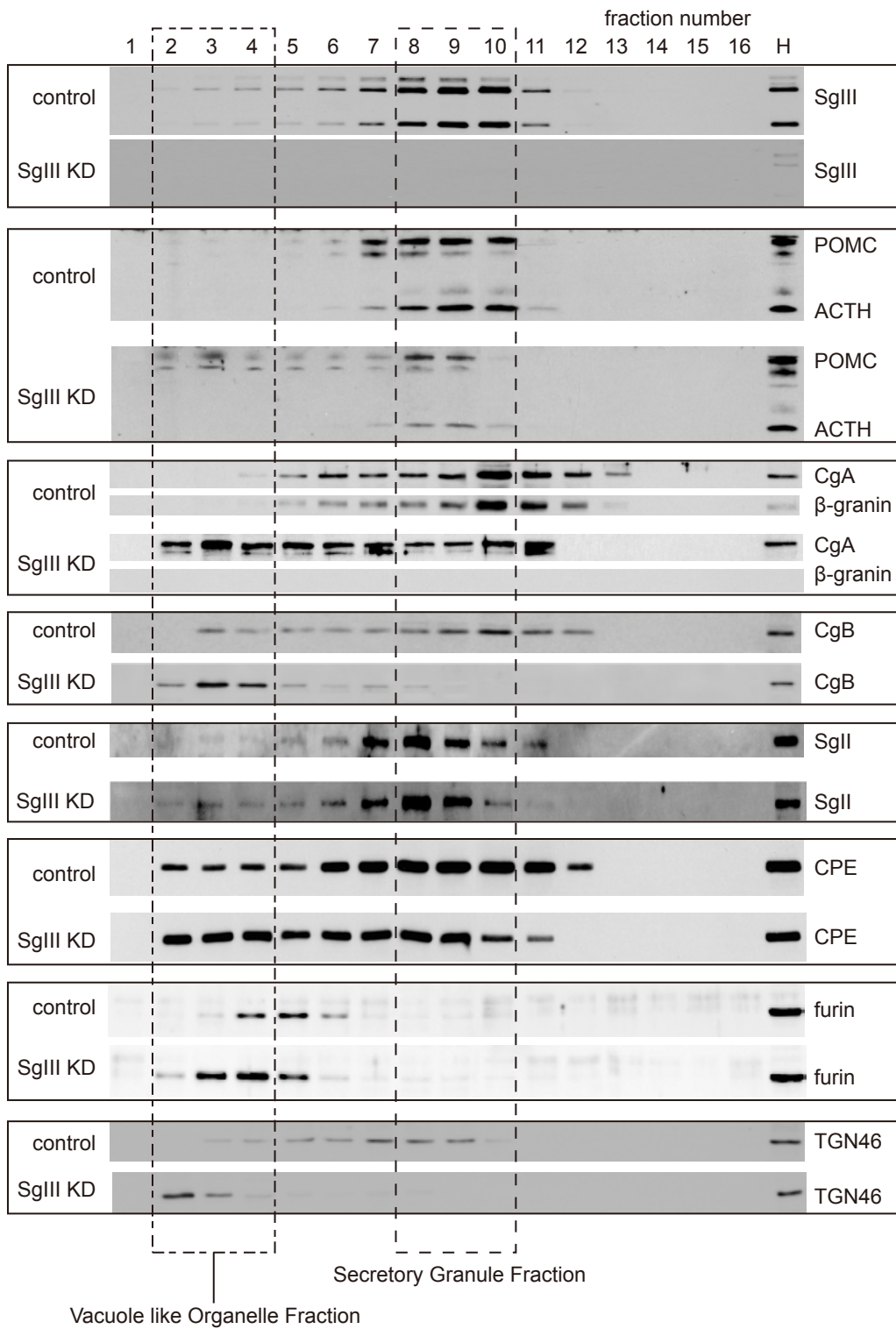




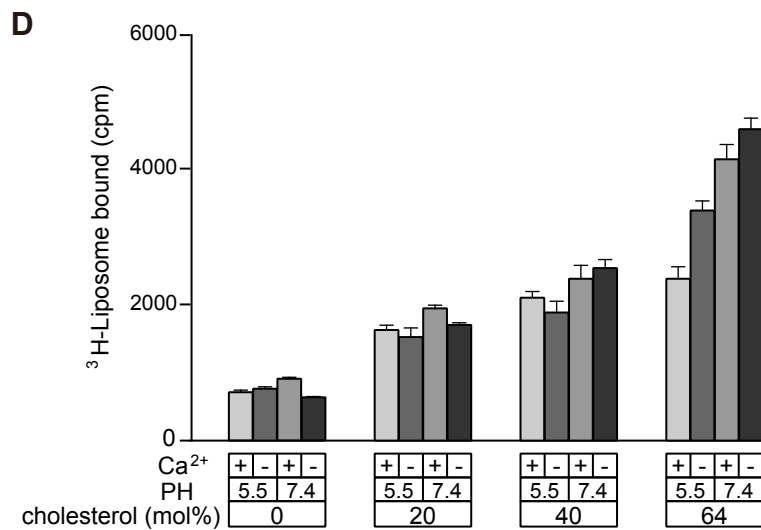
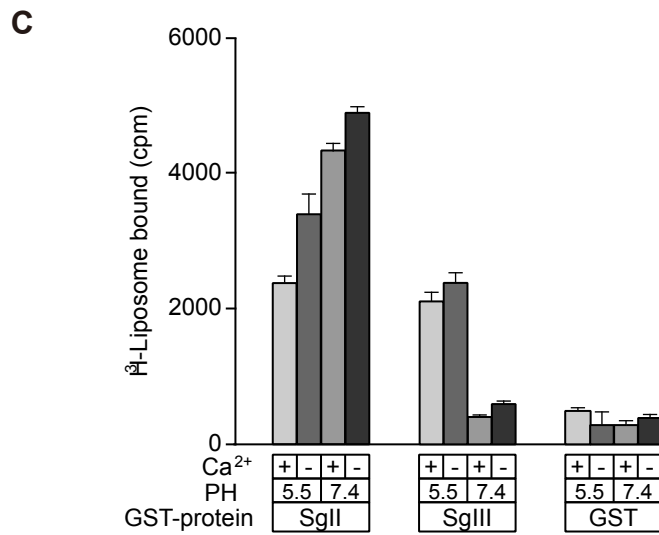
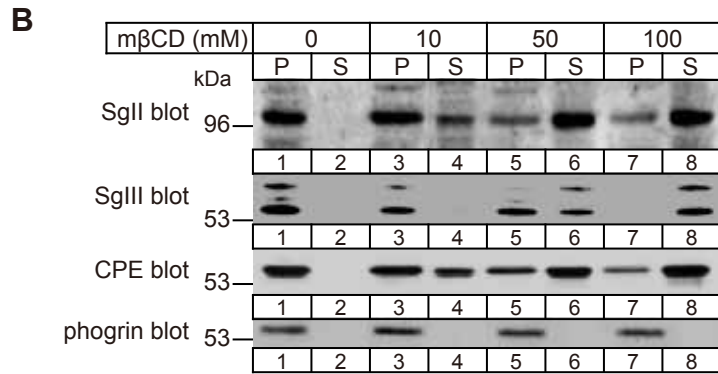
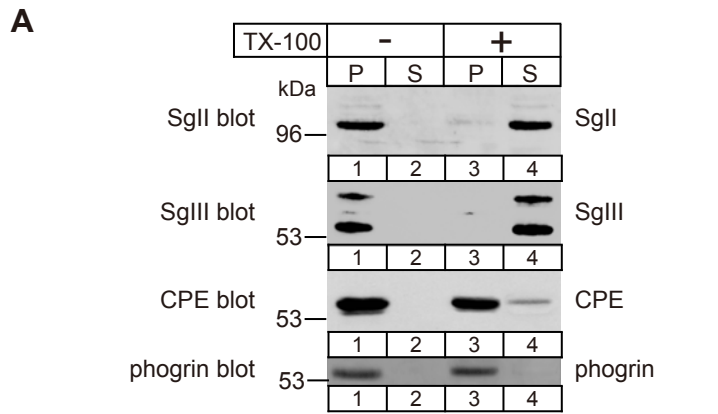
Sun et al., Figure 4



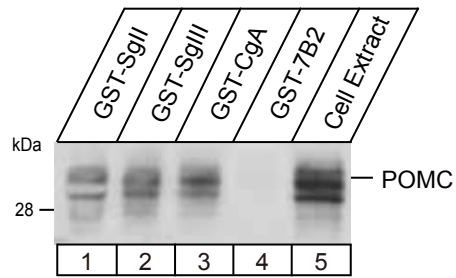
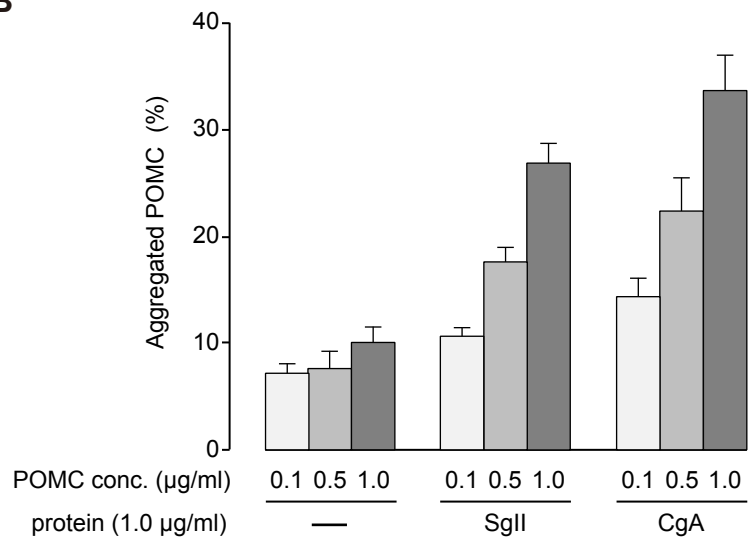
Sun et al., Figure 5

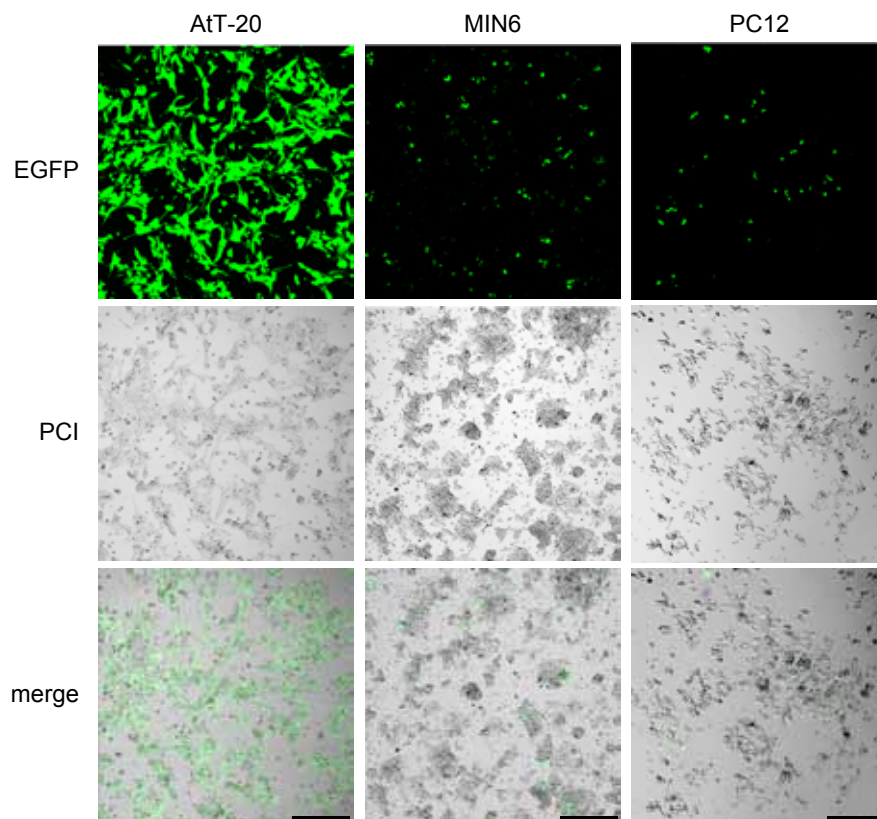


Sun et al., Figure 6



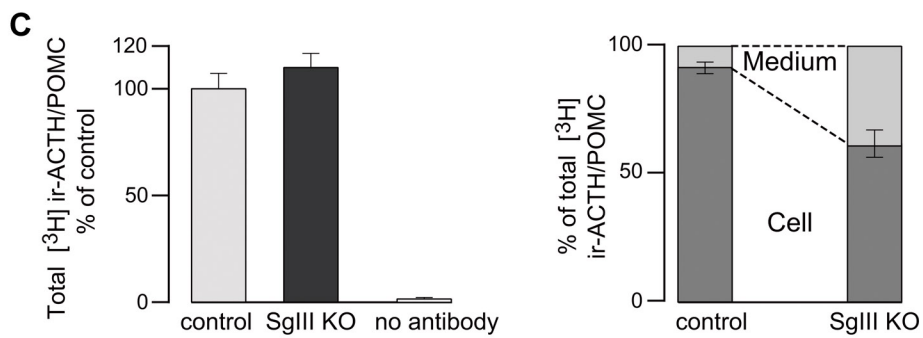
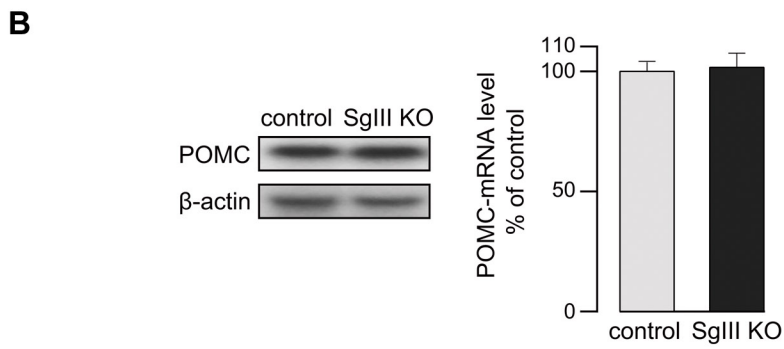
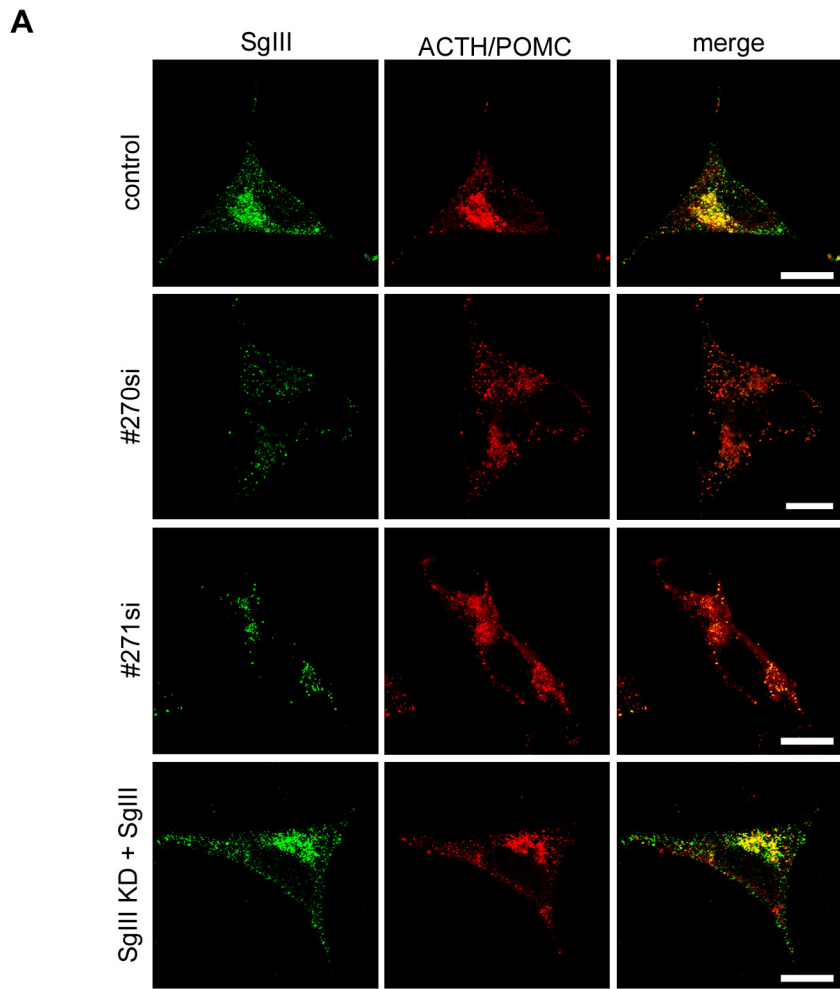
Sun et al., Figure 7

A**B**

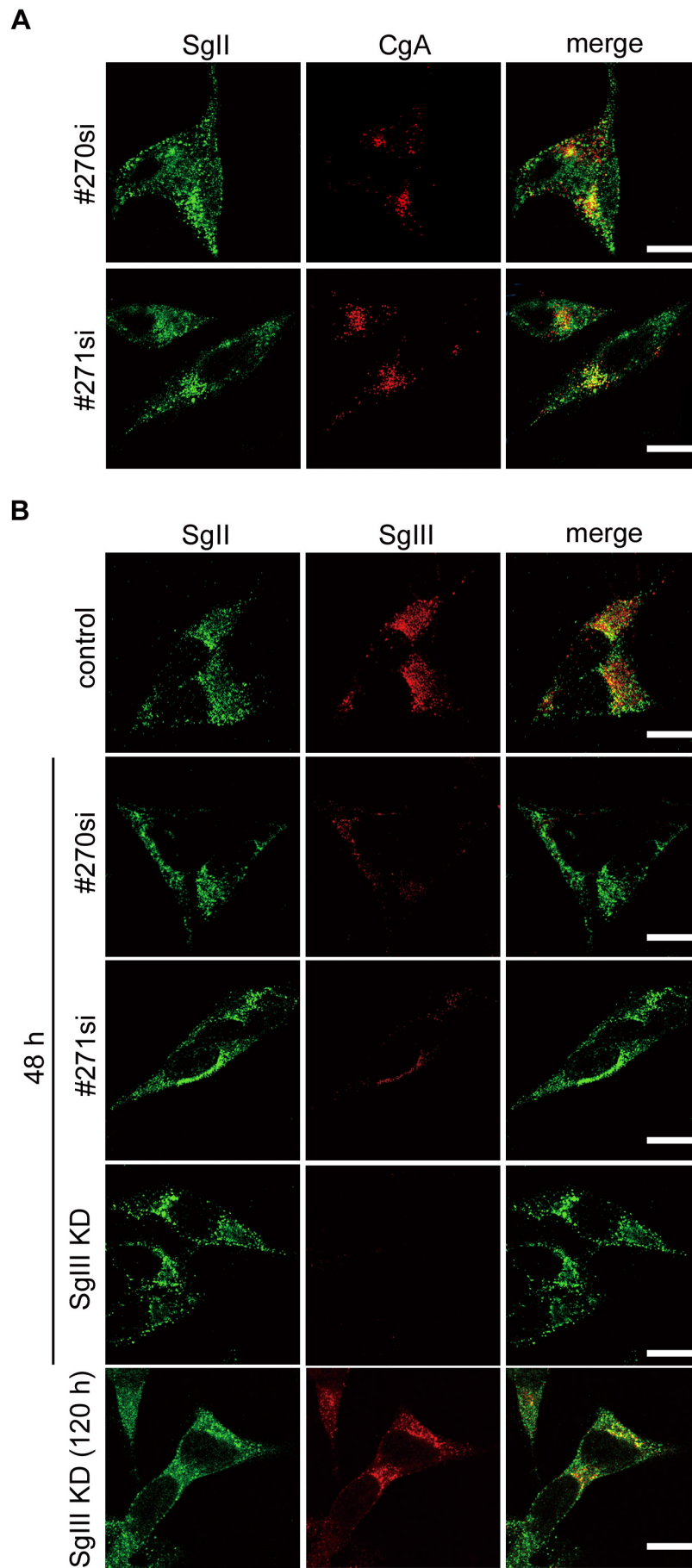


Supporting Information

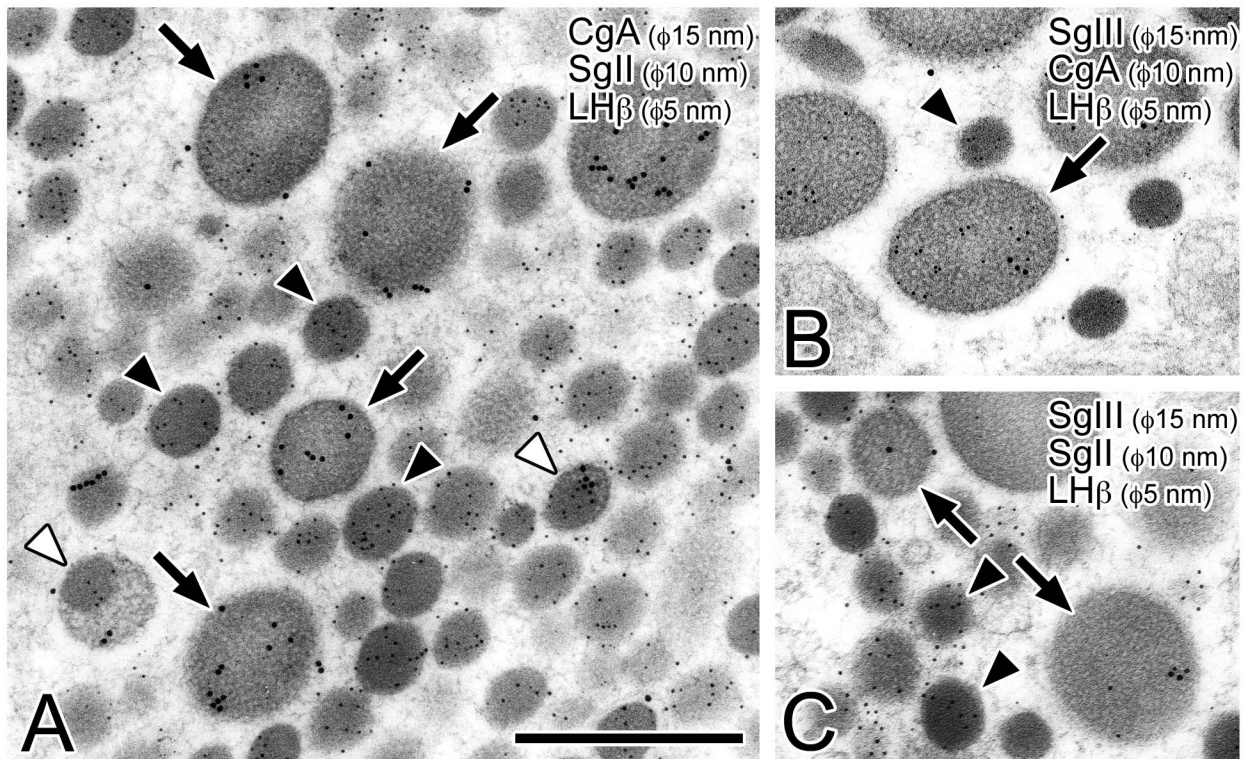
Figure S1



Supporting Information Figure S2



Supporting Information
Figure S3



Supporting Information

Figure S4